# Greenhouse gases simulations and Inversion

Xiao-Ming Hu (xhu@ou.edu)
https://caps.ou.edu/xhu/

Center for Analysis and Prediction of Storms
University of Oklahoma

Sep 30, 2024, MET 3513 Atmospheric chemistry
July 2025, ShengYang camp

# Motivations: global warming, extreme weather

GLOBAL CHANGE &

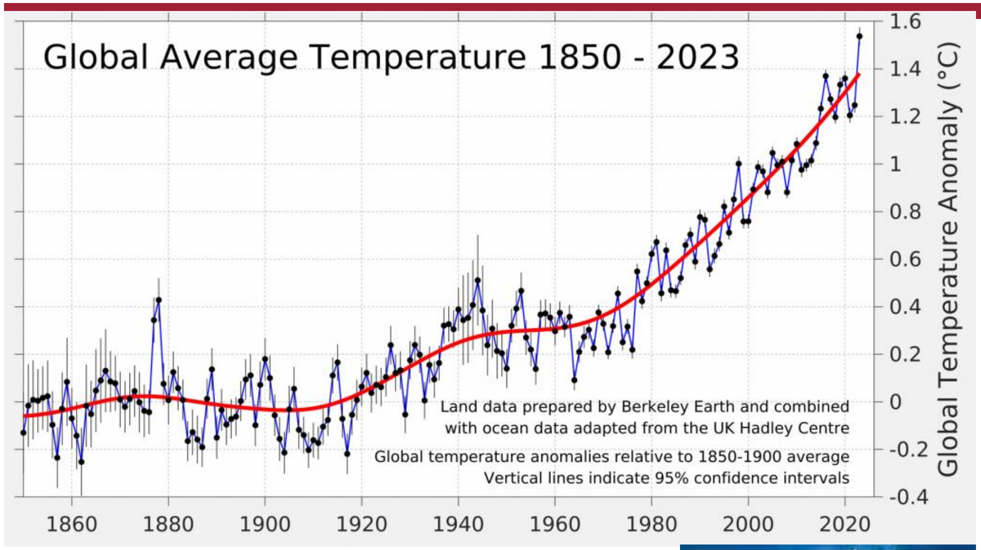



# Trend of $CO_2$

Remote sensing

In situ

In situ

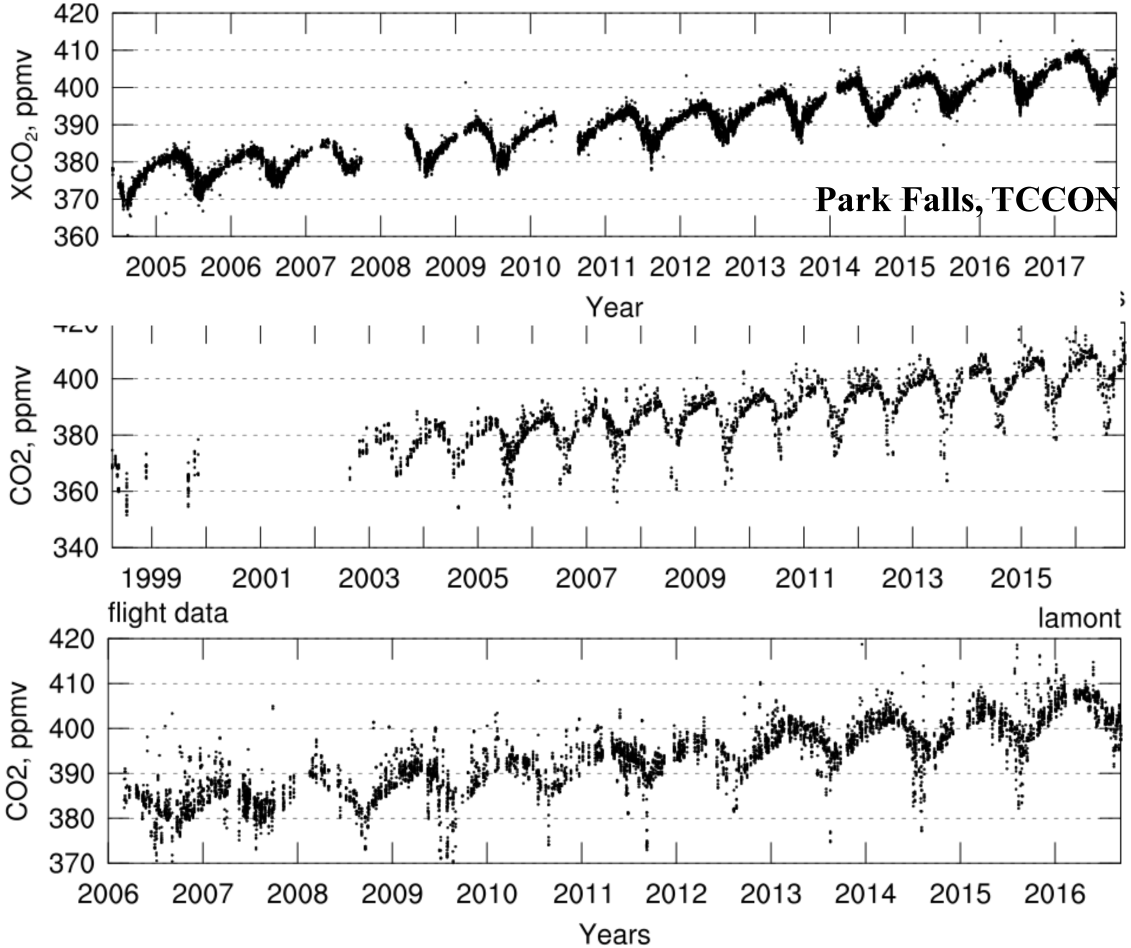


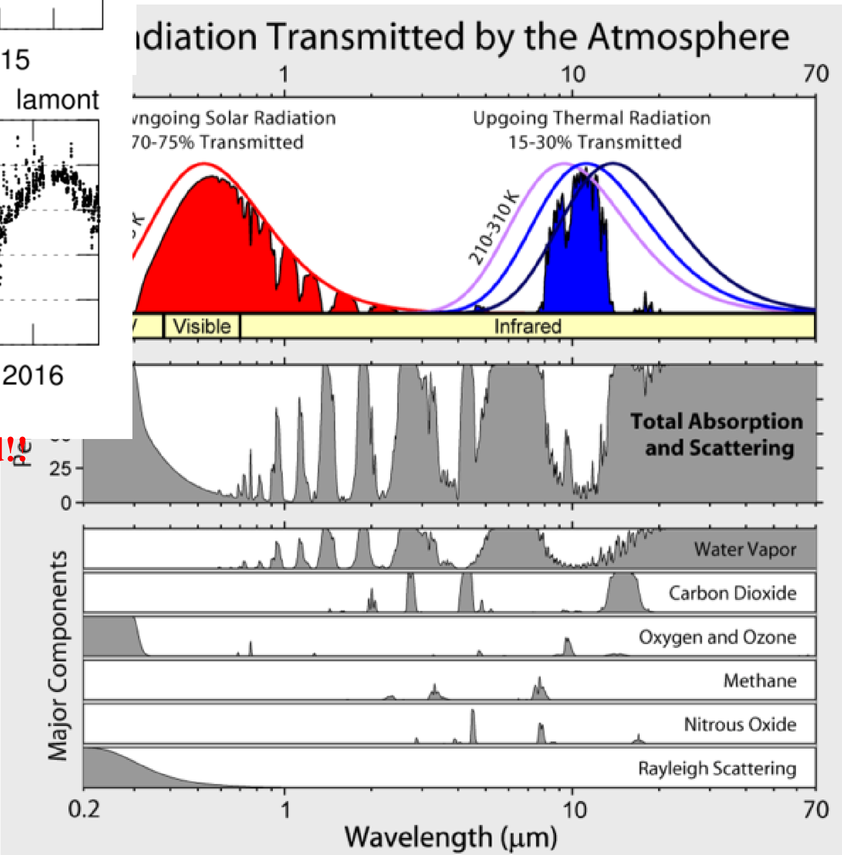


Global warming controversial? Look at $CO_2$ trend!!

# Motivations: greenhouse gas effect

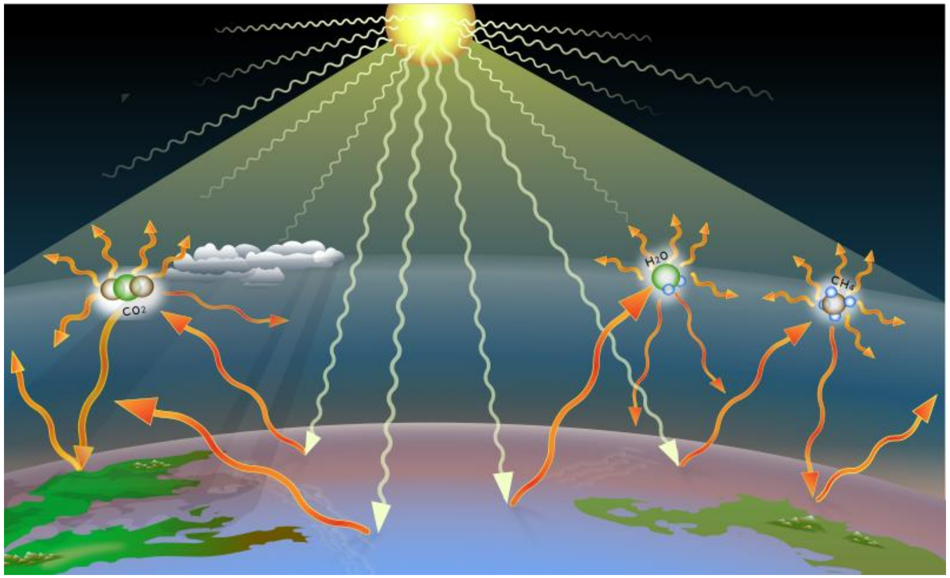

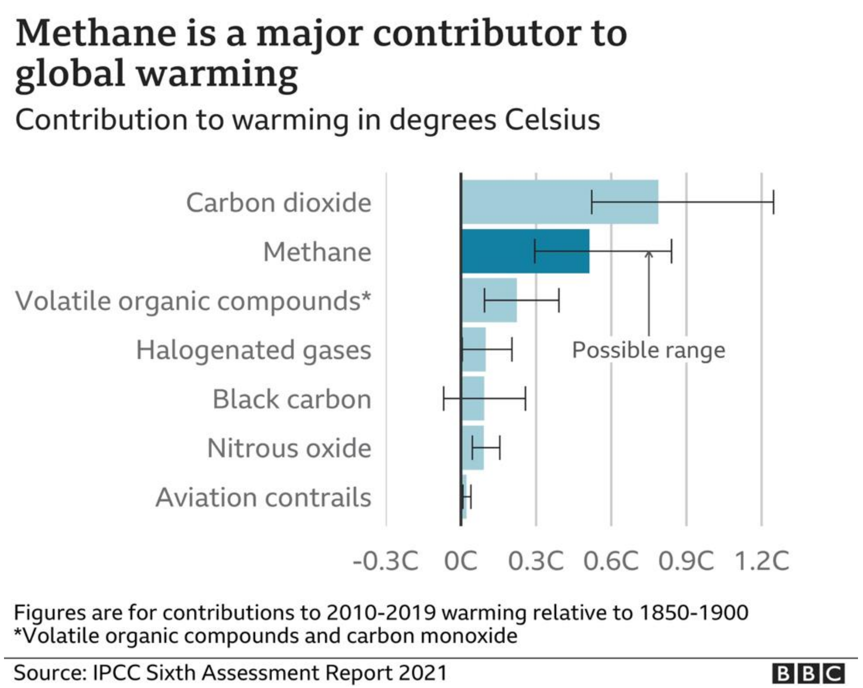


- $CH_4/CO_2$ sources are unknown
- Instruments are either too expensive or spatiotemporal coverage is not enough
- Uncertainties of forward simulation are large, which prevents accurate inversion

1. 3D WRF-$CO_2$ simulation

Over US and China

2. Multi-Model investigation of Haze Pollution
3. WRF-GHG for both $CO_2$ and $CH_4$ simulation
4. CH4 inversion

# Global $CO_2$ sources and sinks

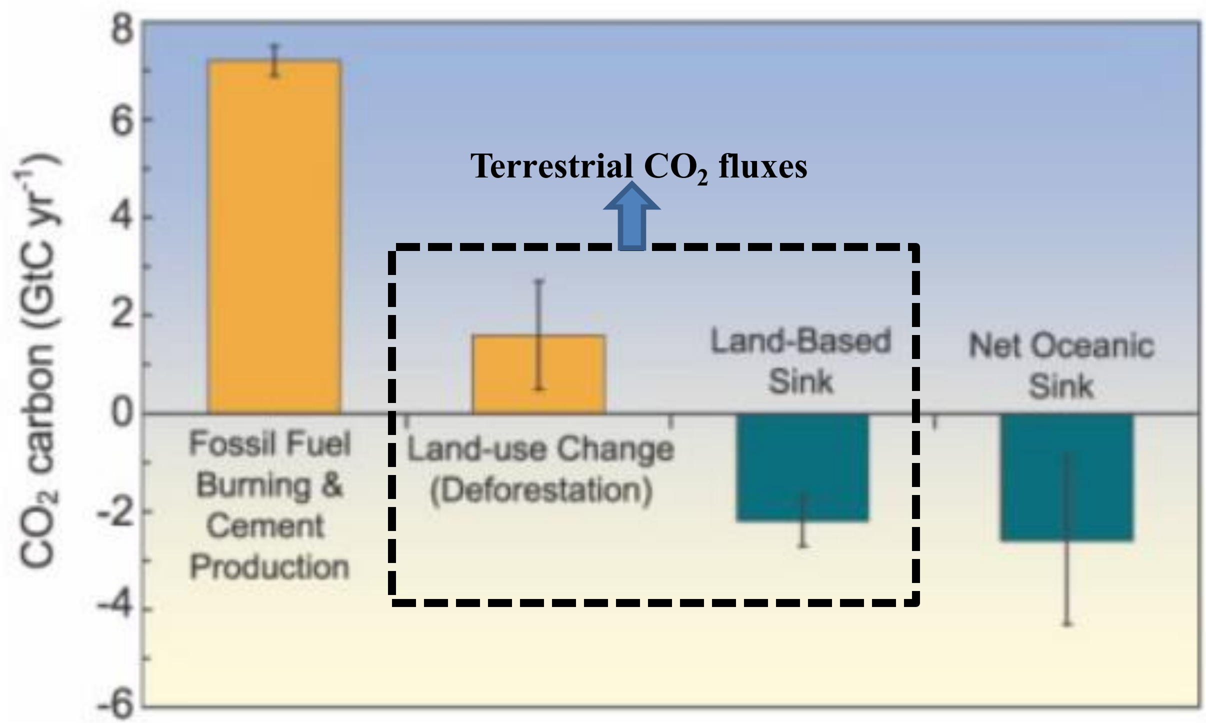


IPCC (2007)

**Uncertainties of terrestrial $CO_2$ fluxes are large**

# Terrestrial $CO_2$ fluxes in different regions

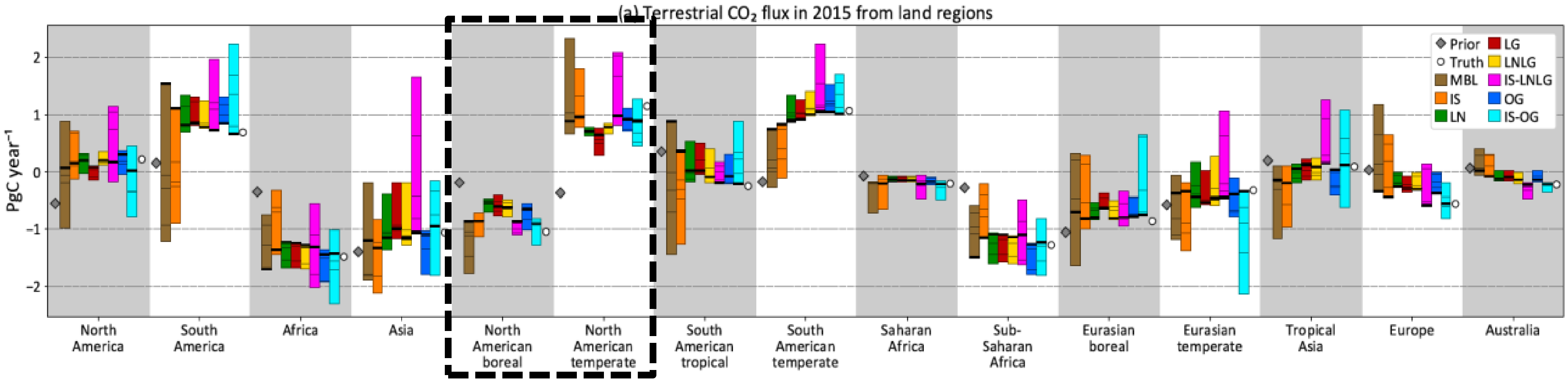


(Sourish Basu et al., 2018)

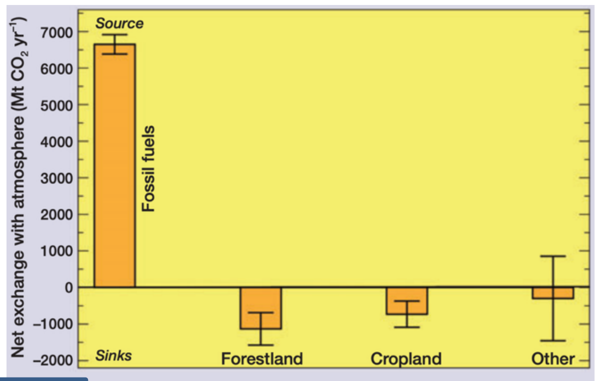


*North American $CO_2$ sources and sinks, circa 2010. The foss*

King et al., 2012

**Uncertainties in each region/plant function are large too**

# Weather-biosphere online-coupled WRF-VPRM

- Vegetation Photosynthesis and Respiration Model (VPRM) (Xiao et al., 2004; Mahadevan et al., 2008; Ahmadov et al., 2007)

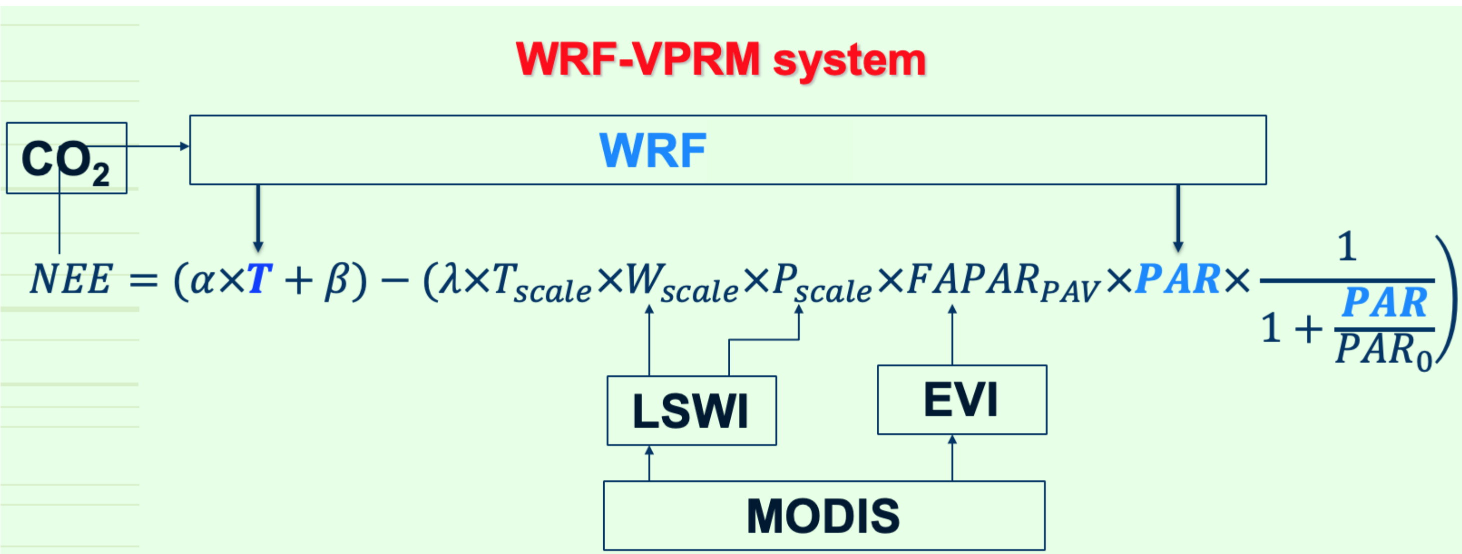


$$NEE = (\alpha \times \boldsymbol{T} + \beta) - \left(\lambda \times T_{scale} \times W_{scale} \times P_{scale} \times FAPAR_{PAV} \times \boldsymbol{PAR} \times \frac{1}{1 + \frac{\boldsymbol{PAR}}{PAR_0}}\right)$$

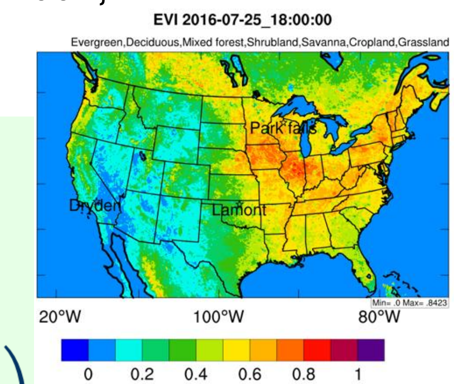


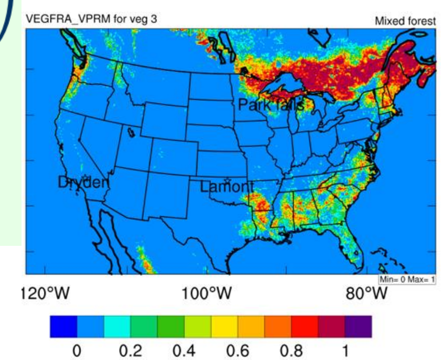


$\alpha$, $\beta$, $\lambda$, $PAR_0$ need flux data calibration

More details in Hu et al., 2020, JAMES

# Implemented parameters from Hilton et al. (2013)

**Calibrated using eddy covariance tower data over North America**

| | Evergreen forest | Deciduous forest | Mixed forest | Shrub | Savanna | Crop | Grass |
|---|---|---|---|---|---|---|---|
| $PAR_0$ | 745.306 | 514.13 | 419.5 | 590.7 | 600 | 1074.9 | 717.1 |
| $\lambda$ | 0.13 | 0.1 | 0.1 | 0.18 | 0.18 | 0.085 | 0.115 |
| $\alpha$ | 0.1247 | 0.092 | 0.2 | 0.0634 | 0.2 | 0.13 | 0.0515 |
| $\beta$ | 0.2496 | 0.843 | 0.27248 | 0.2684 | 0.3376 | 0.542 | -0.0986 |

**And other minor changes to VPRM in WRF**

# Downscaling in 2016 from CarbonTracker

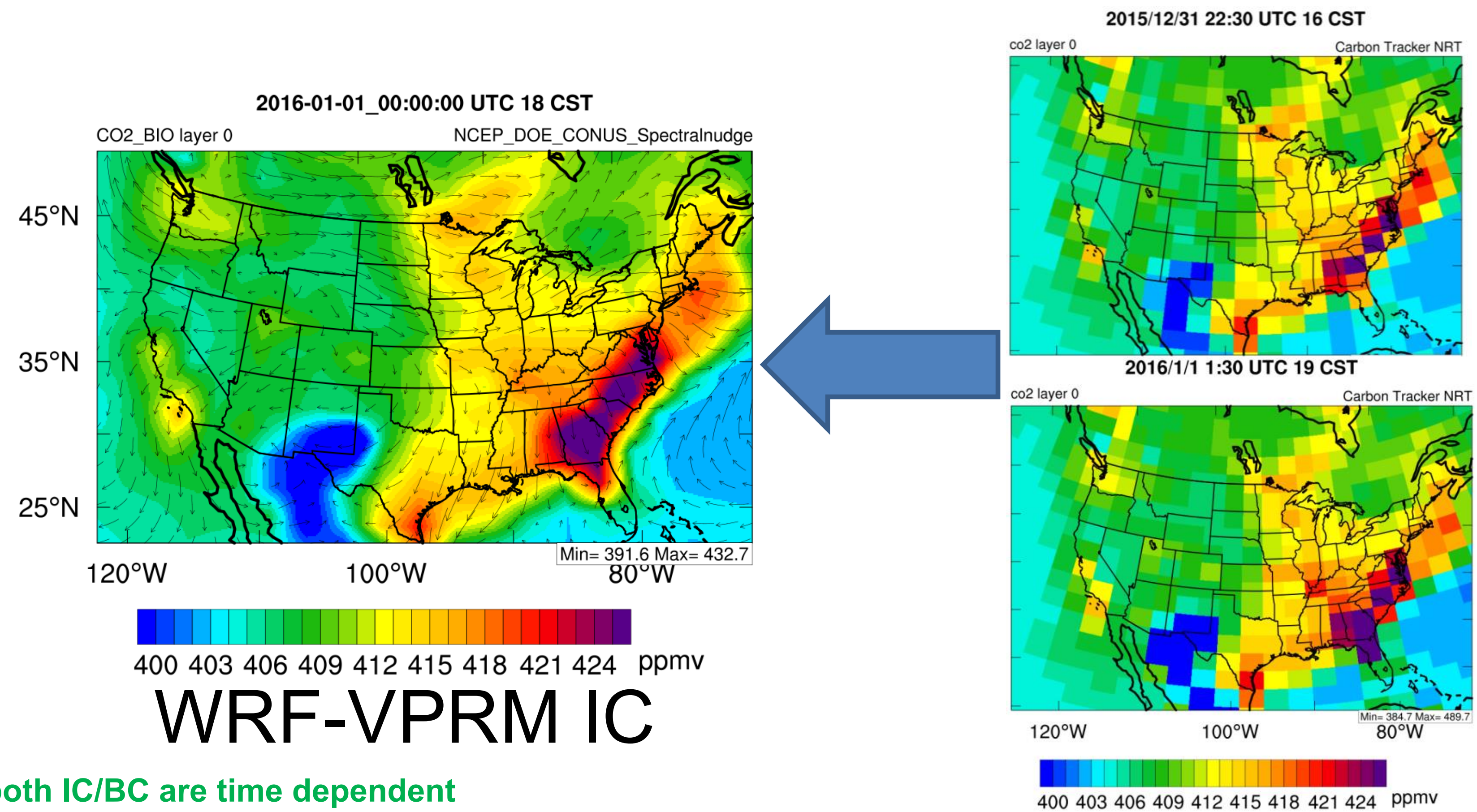


WRF-VPRM IC

**Point 1: both IC/BC are time dependent**
**Point 2: resolution of WRF-VPRM is much higher, adequate to investigate impact of weather**

# configuration for WRF-VPRM downscaling

| Short wave radiation | Dudhia |
|---|---|
| Long wave radiation | rapid radiative transfer model (RRTM) |
| Boundary layer | YSU |
| Microphysics | Morrison |
| Cumulus | Grell-Freitas |
| Land surface model | NOAH |
| Vertical levels | 47 |
| Horizontal resolution | 12 km × 12 km with 266×443 grid points |
| Time step | 60 seconds |
| Meteo initial and lateral boundary conditions | NCEP/DOE Reanalysis 2 (R2) |
| $CO_2$ initial and lateral boundary conditions | **CarbonTracker** global simulation 3°×2° outputs |
| Interior nudging | **Spectral nudging** |
| nudging variables | horizontal wind components, temperature, geopotential |
| nudging coefficient | $3 \times 10^{-5}$ $s^{-1}$ |
| nudging height | above PBL |
| wave number | 5 and 3 in the zonal and meridional directions respectively |
| nudging period | throughout the downscaling simulation |

## Biogenic $CO_2$ fluxes downscaled by WRF-VPRM vs. CarbonTracker posterior fluxes

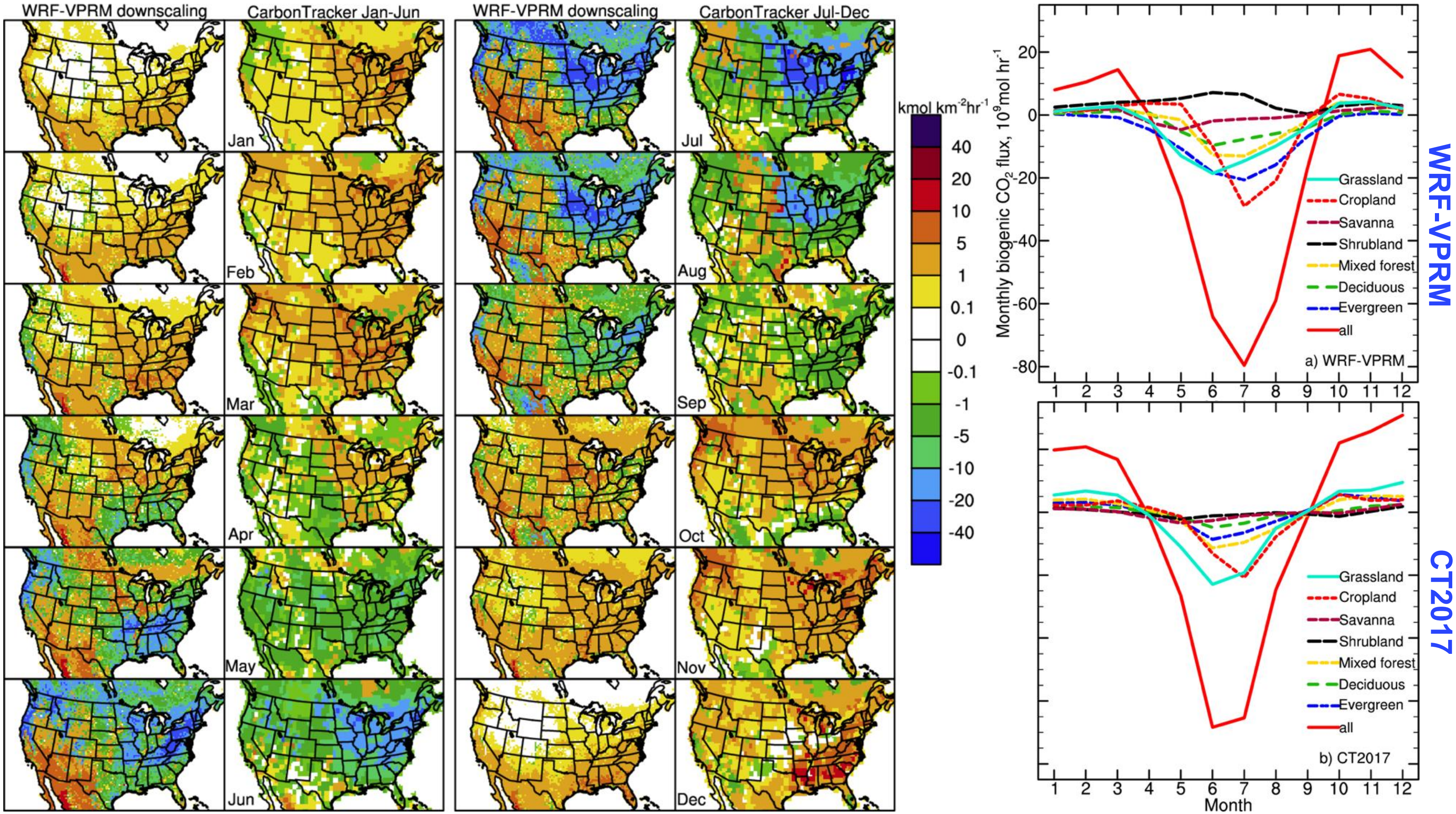

# $XCO_2$ at the 4 TCCON sites

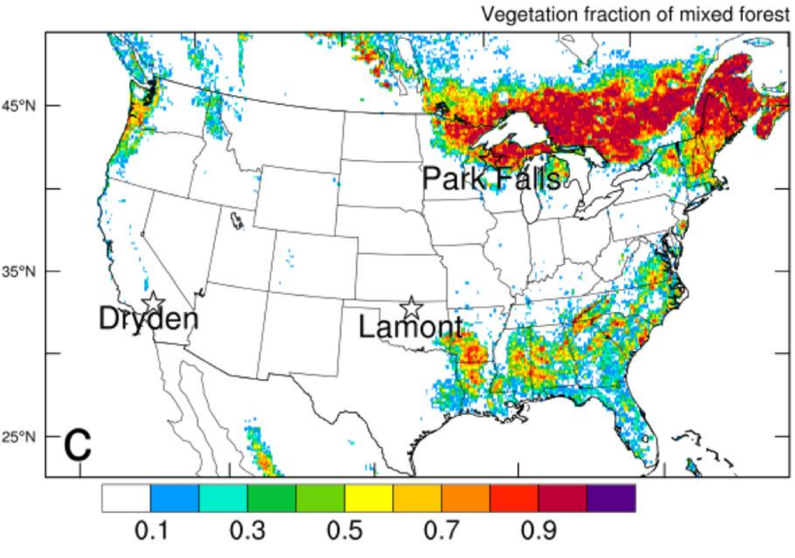


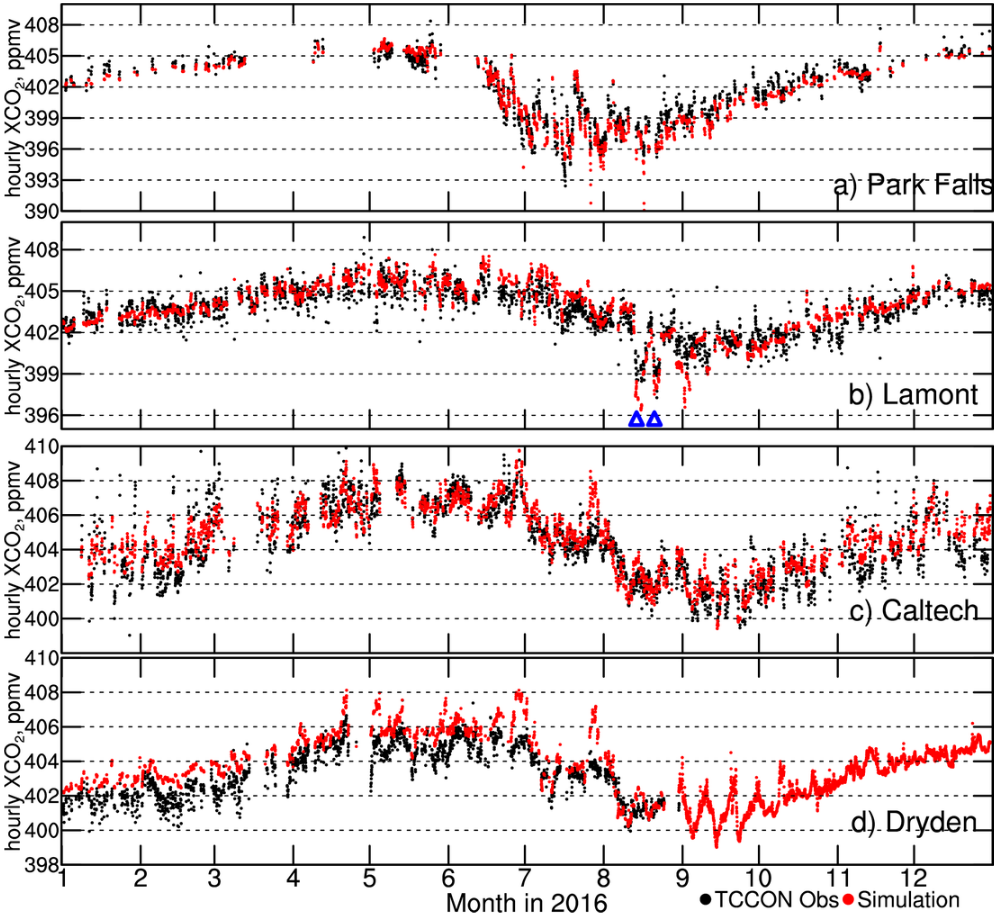


Bias in western boundary?
Bias in anthropogenic emission?

captures the seasonal and some episodic variation of $XCO_2$.

# Evaluation of CT2017

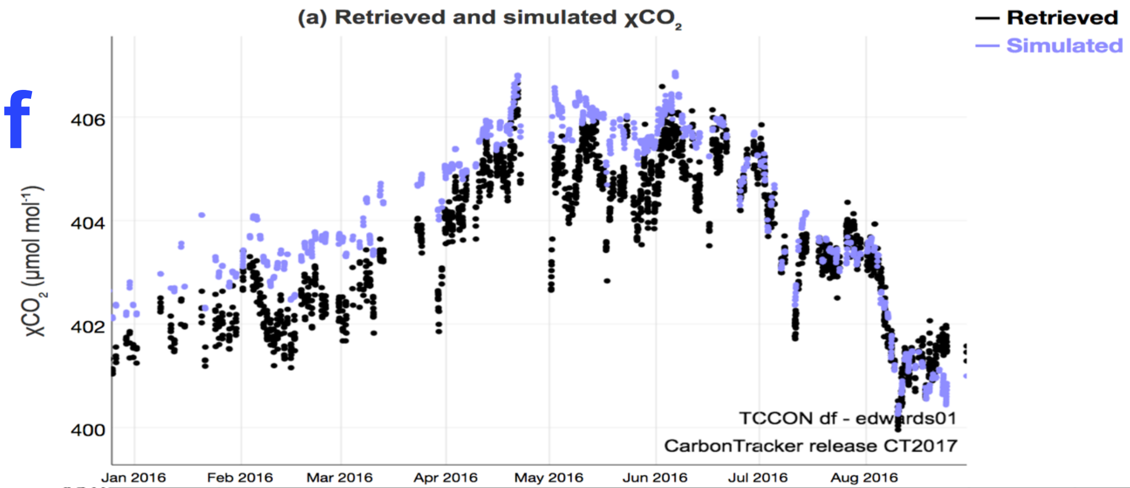


# Evaluation of WRF-VPRM

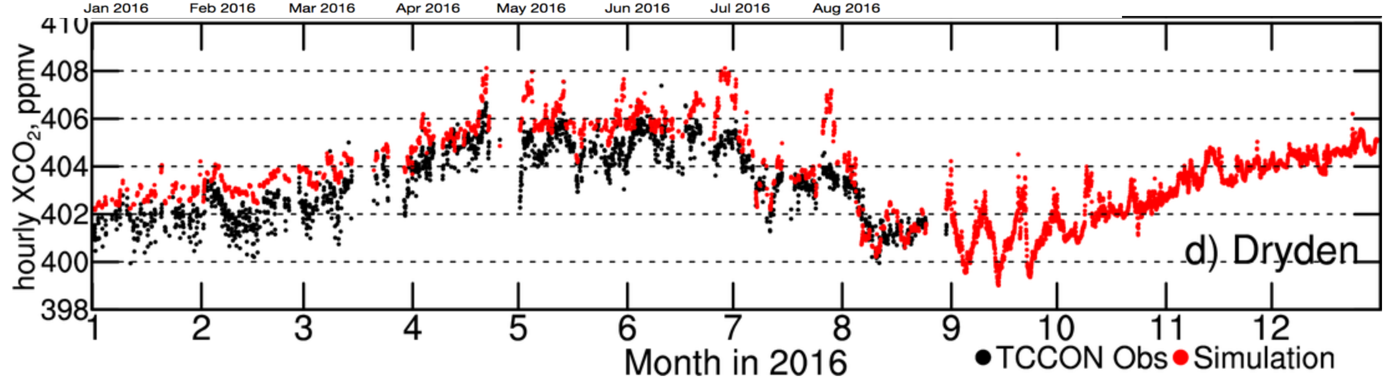


Thus, bias in western boundary partially contributed to WRF-VPRM bias?

# Compare with OCO-2; individual contributions

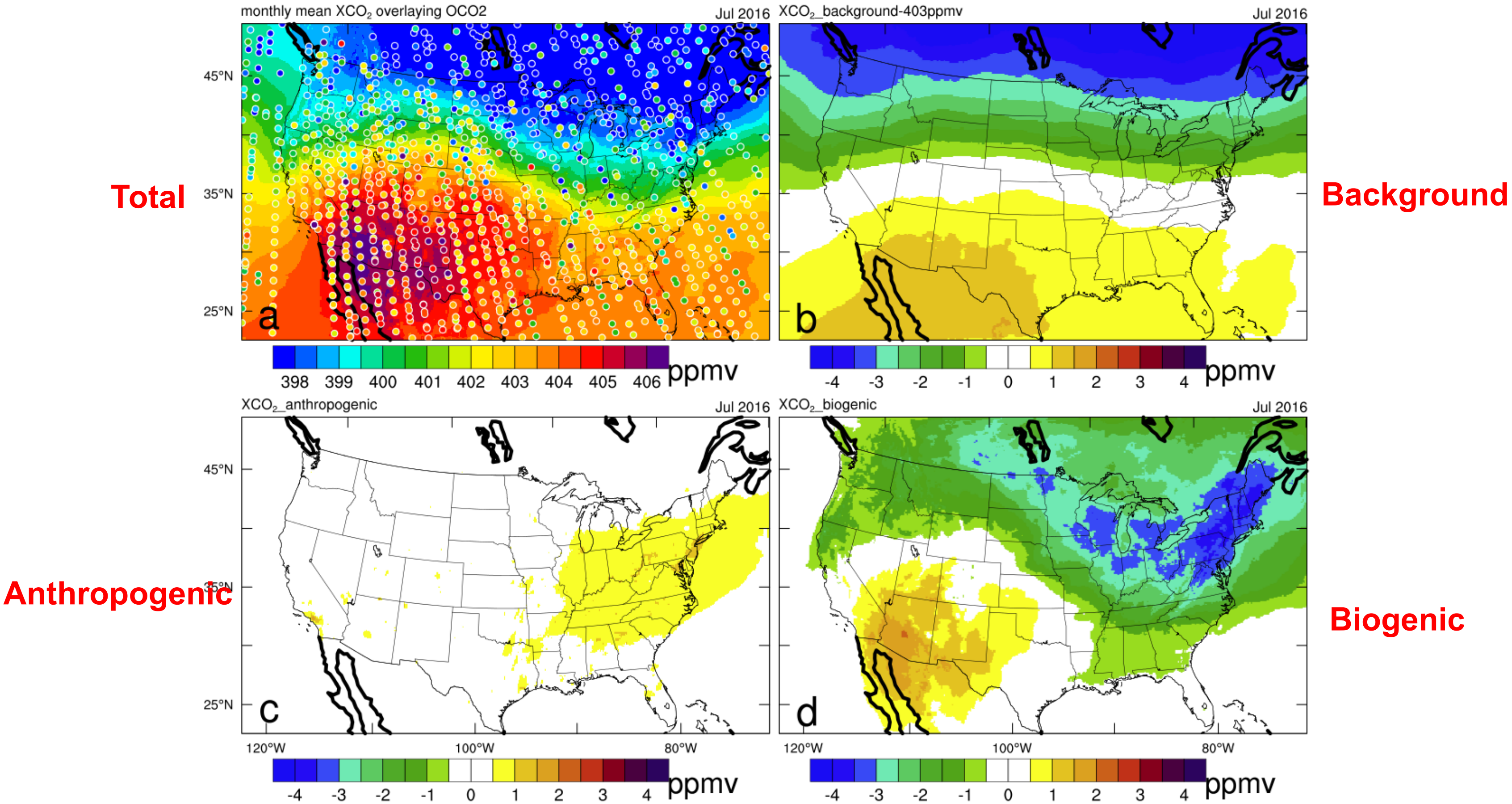

# Compare with OCO-2, individual cases

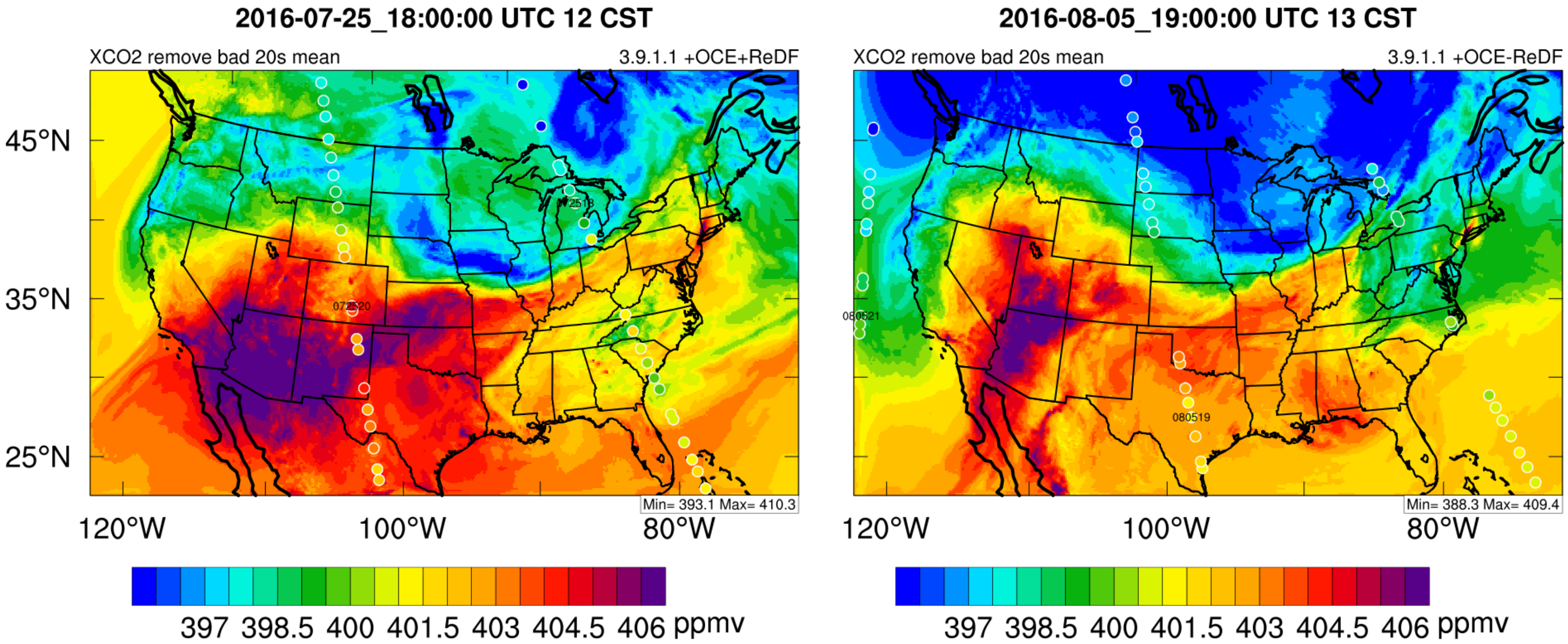

# Case study, Aug 5
# OCO-2 underpass

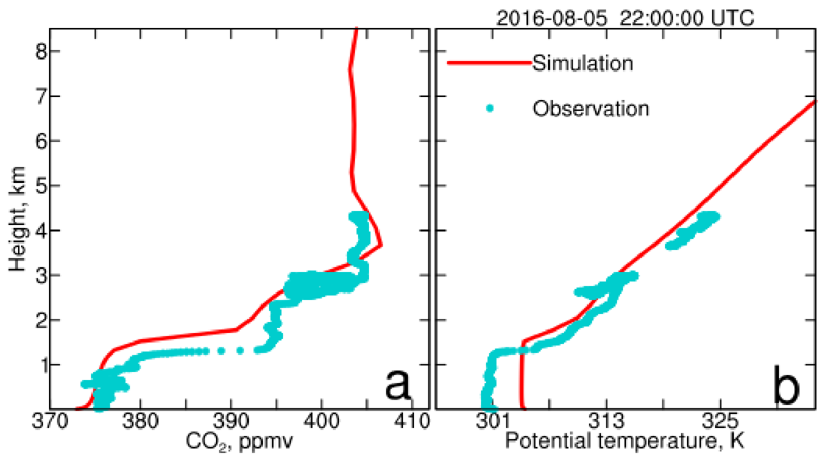


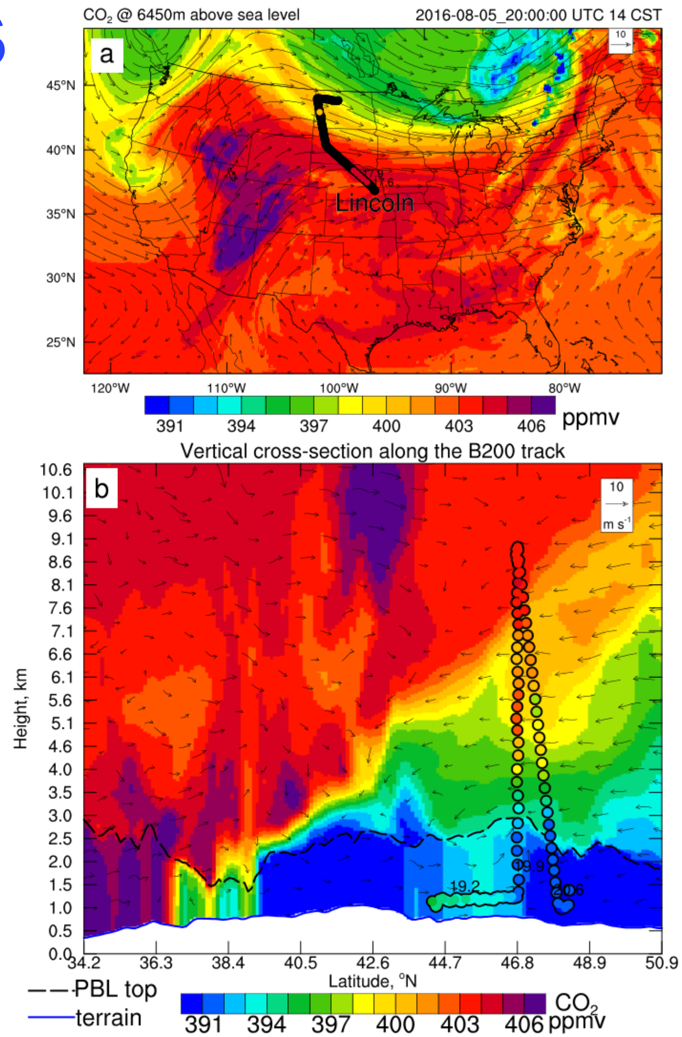

# Summary

1. Calibrated VPRM parameters from Hilton et al [2013] are implemented into WRF-VPRM
2. WRF-VPRM reasonably captures monthly variation of $XCO_2$ and episodic variations due to frontal passages
3. The downscaling also successfully captures the horizontal $CO_2$ gradients across fronts, as well as vertical $CO_2$ contrast across the boundary layer top.

# Terrestrial $CO_2$ fluxes in different regions

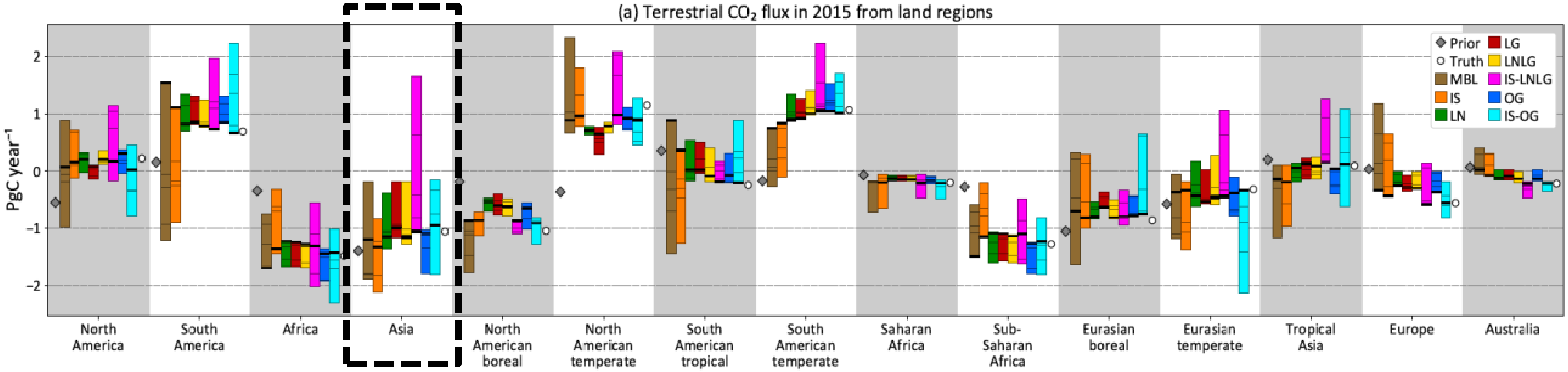


(Sourish Basu et al., 2018)

Uncertainties in each region are large too

Asia is $CO_2$ sink!!

# Northeast China: a major $CO_2$ sink

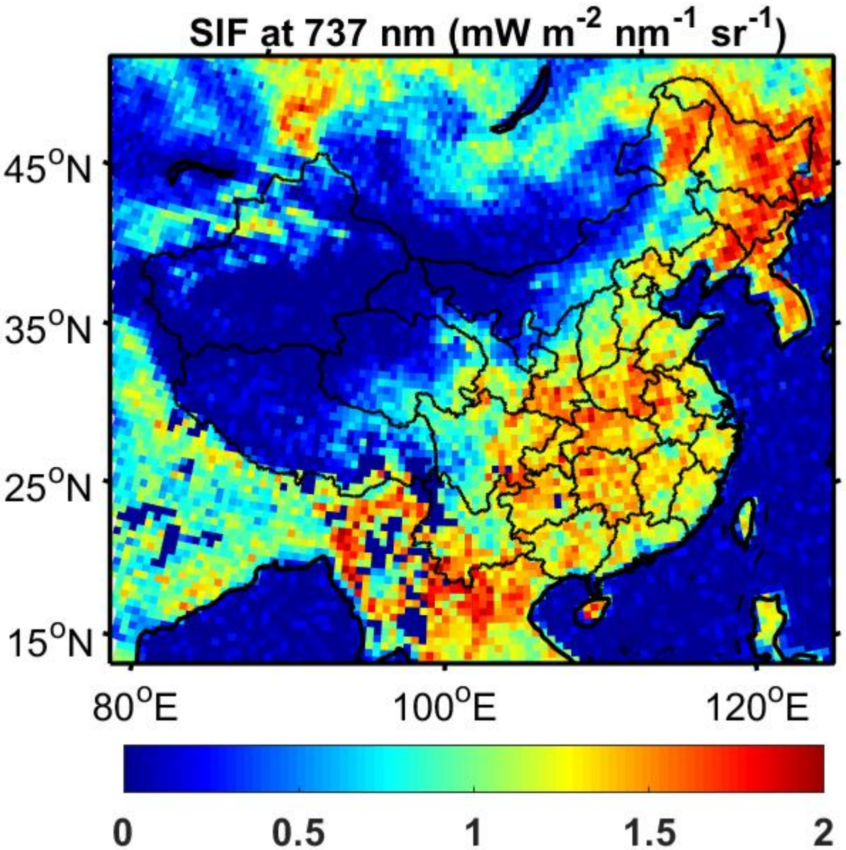


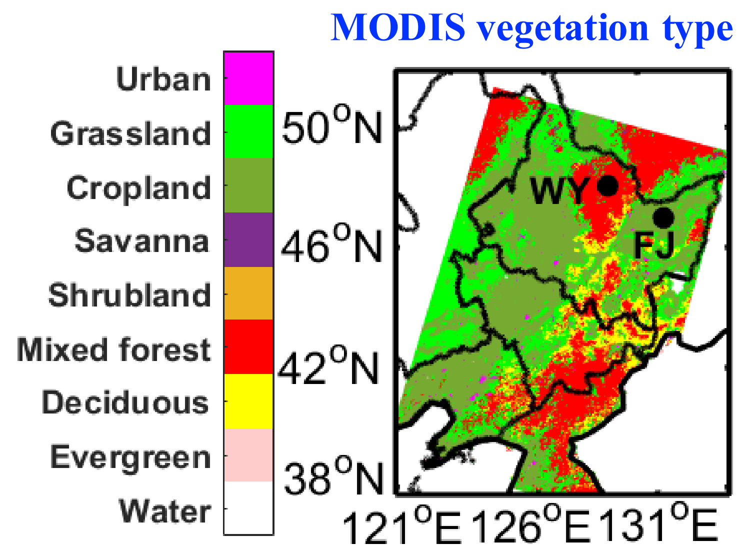


Mixed forest and cropland dominate in Northeast China
Crop area is still increasing!!

SIF: Sun-induced Fluorescence, proportional to photosynthesis

# Long-term tower measurements, focusing on 2016

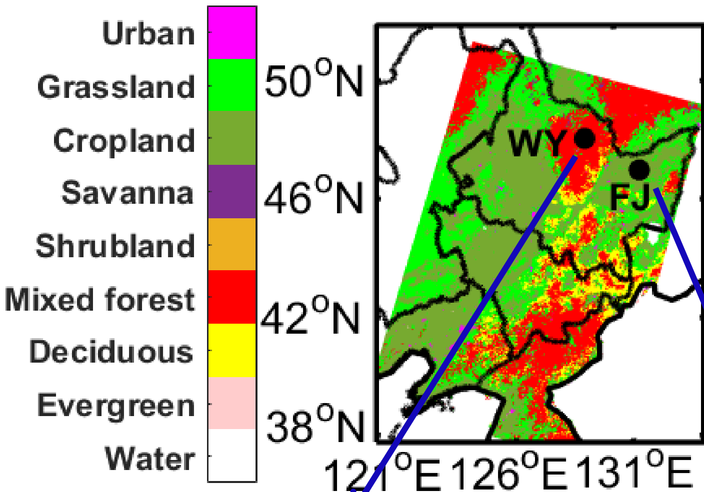


- **Observational parameters:**
  1) Hourly mean $CO_2$ fluxes and concentrations,
  2) wind speed and direction, air temperature
  3) PAR (only at Fujin)

- **Observational period:**
  Fujin: since 2012
  Wuying: since 2014

**Wuying, mixed forest site**
**(131.9385° E, 47.1519° N, 345 m)**

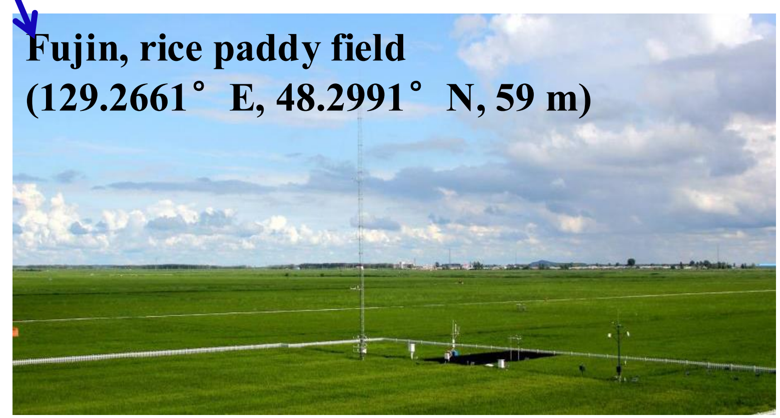

**Fujin, rice paddy field**
**(129.2661° E, 48.2991° N, 59 m)**

# Seasonal variations of $CO_2$ fluxes and concentrations

Fujin (cropland, rice paddy)

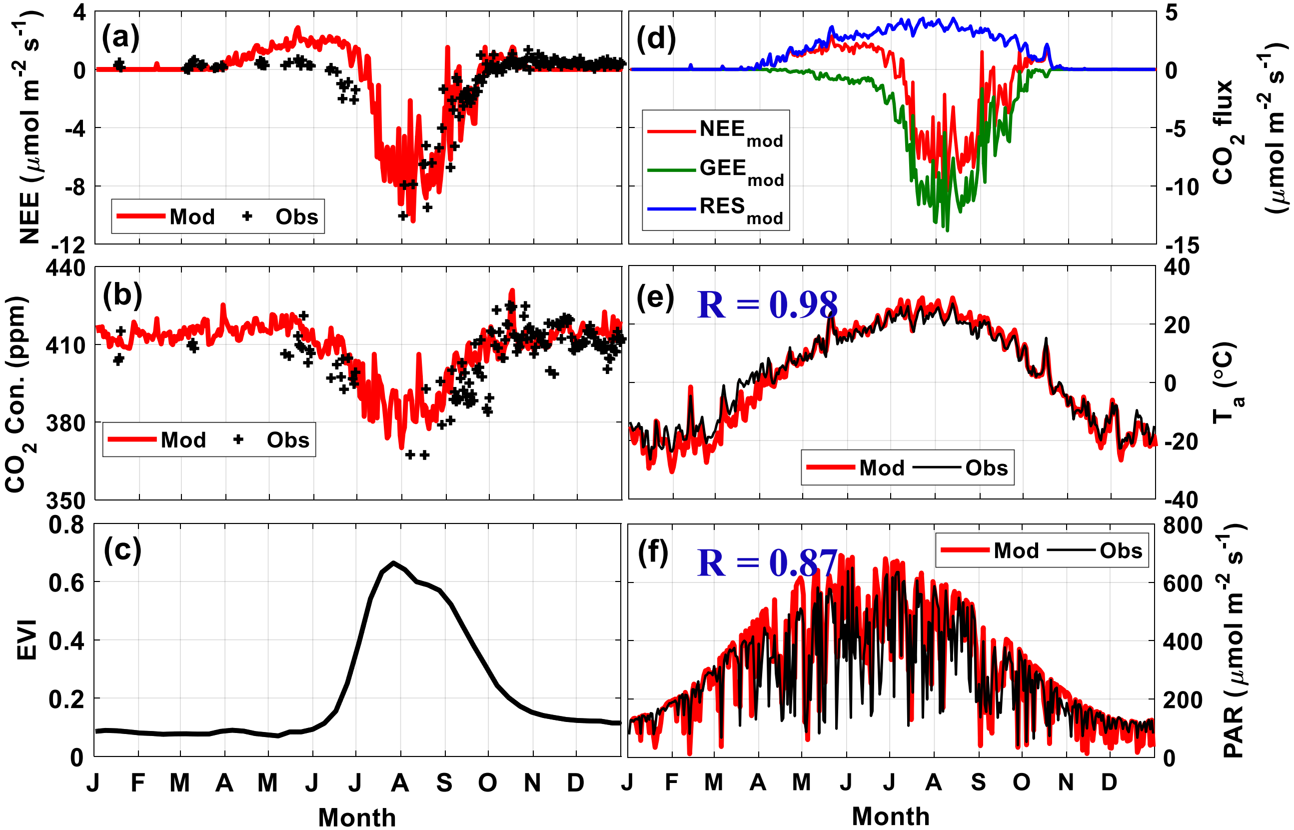


MODIS vegetation type

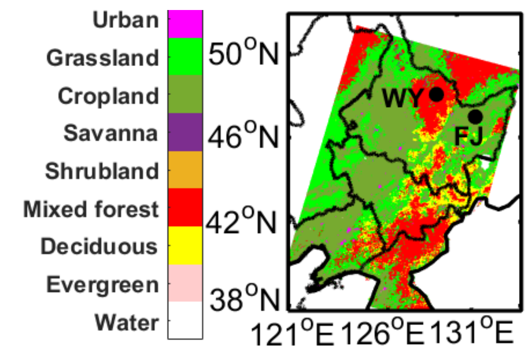

# Bias of terrestrial respiration

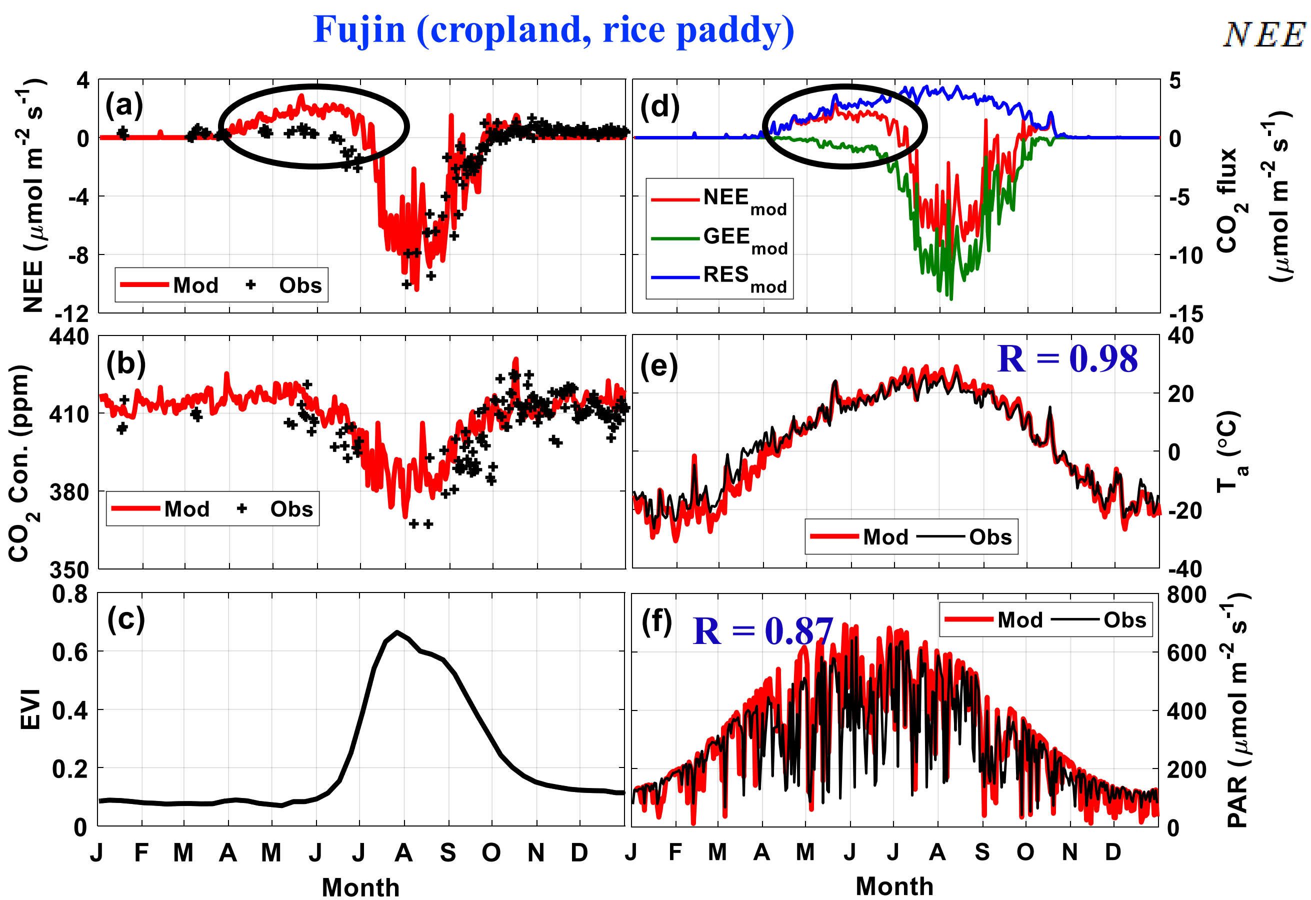


$$NEE = (\alpha \times T + \beta) + GEE$$

largely subjected to the EVI

Ignores leaf mass, involves EVI?

# Seasonal variation of $CO_2$ fluxes and concentrations

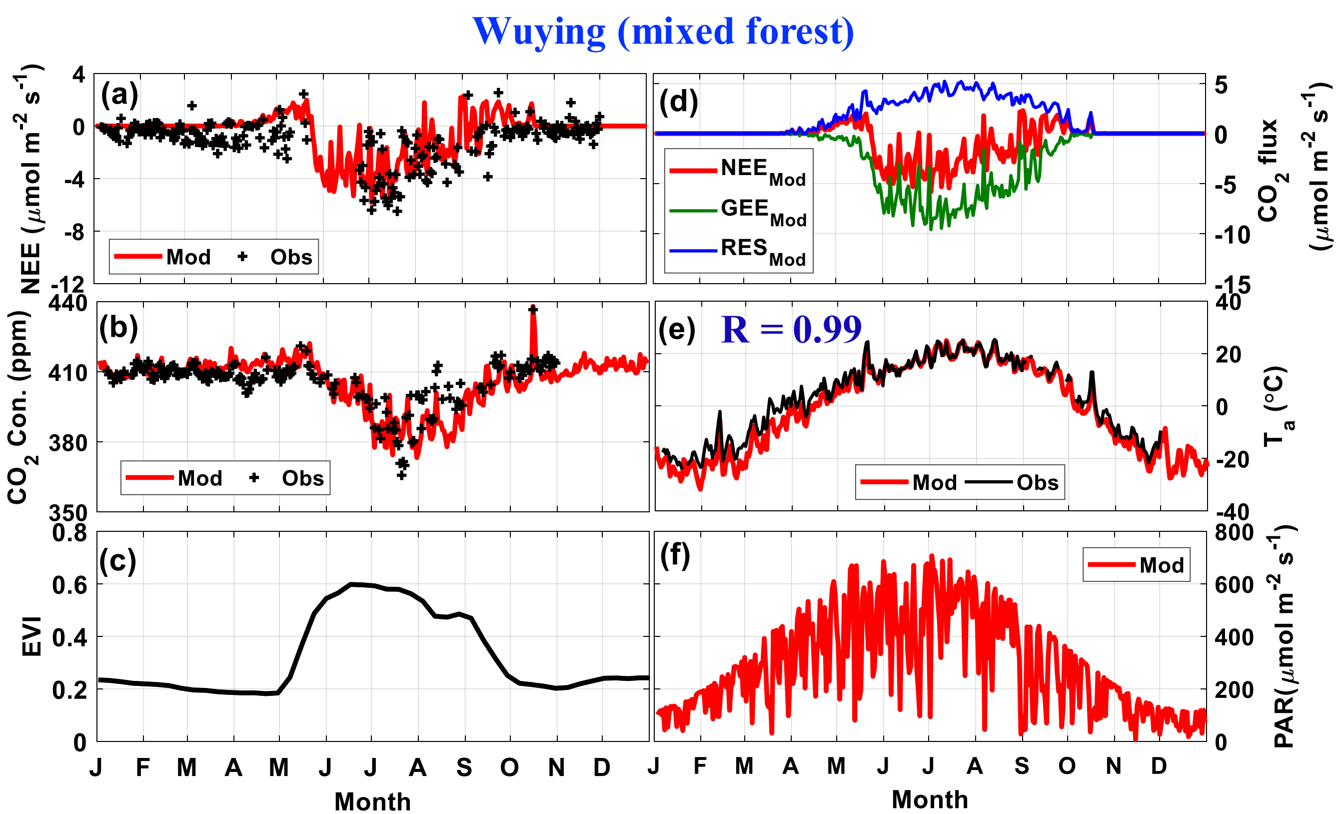


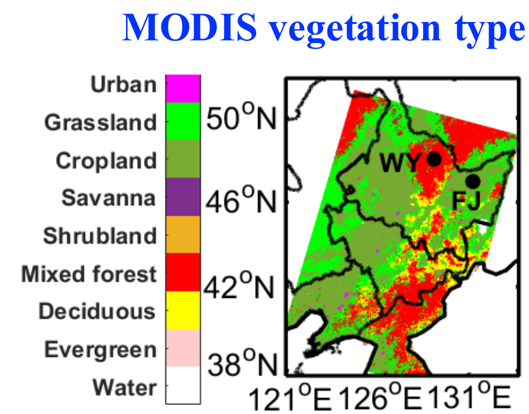

# OCO-2 retrieved $XCO_2$ (L2 Lite Version 9)

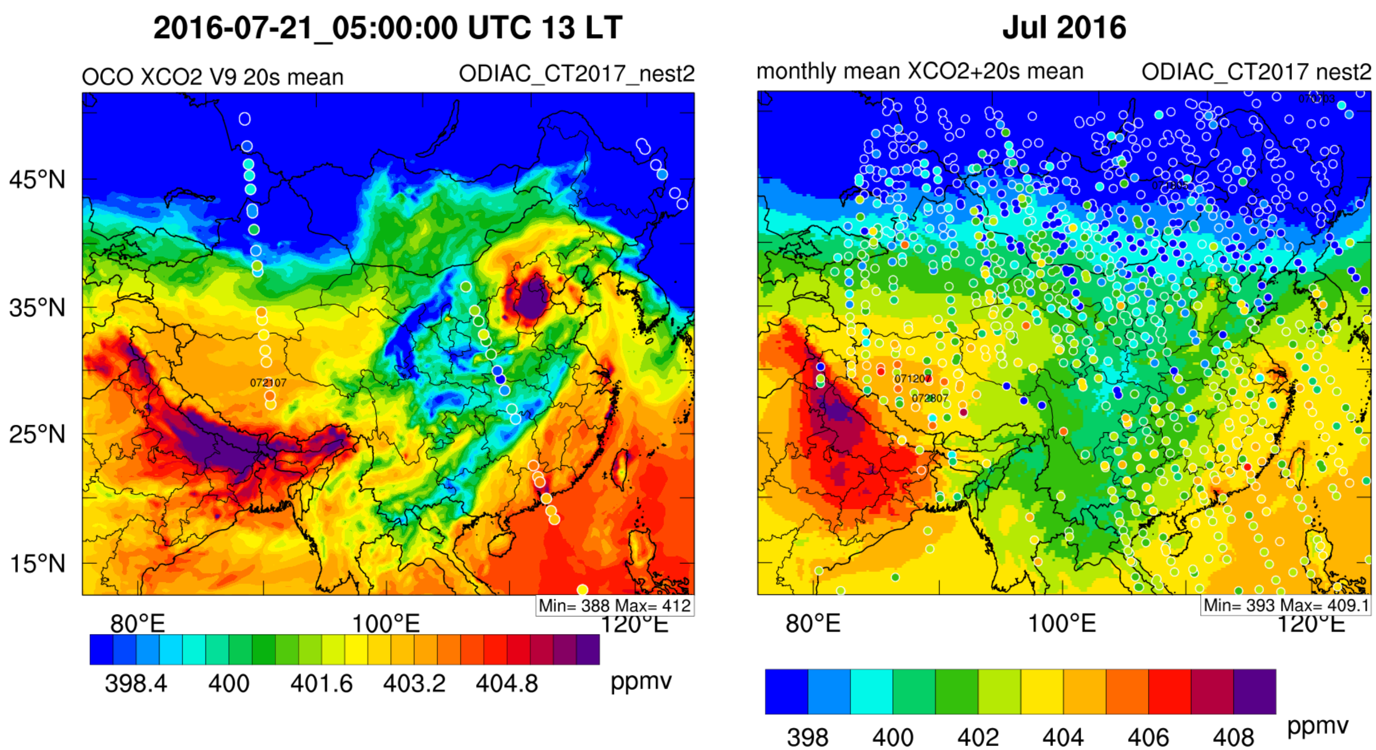


**Advantage: spatiotemporal coverage**
**Disadvantage: interfere with cloud and haze pollution!!**

# Seasonal variation of $XCO_2$ over Northeast China

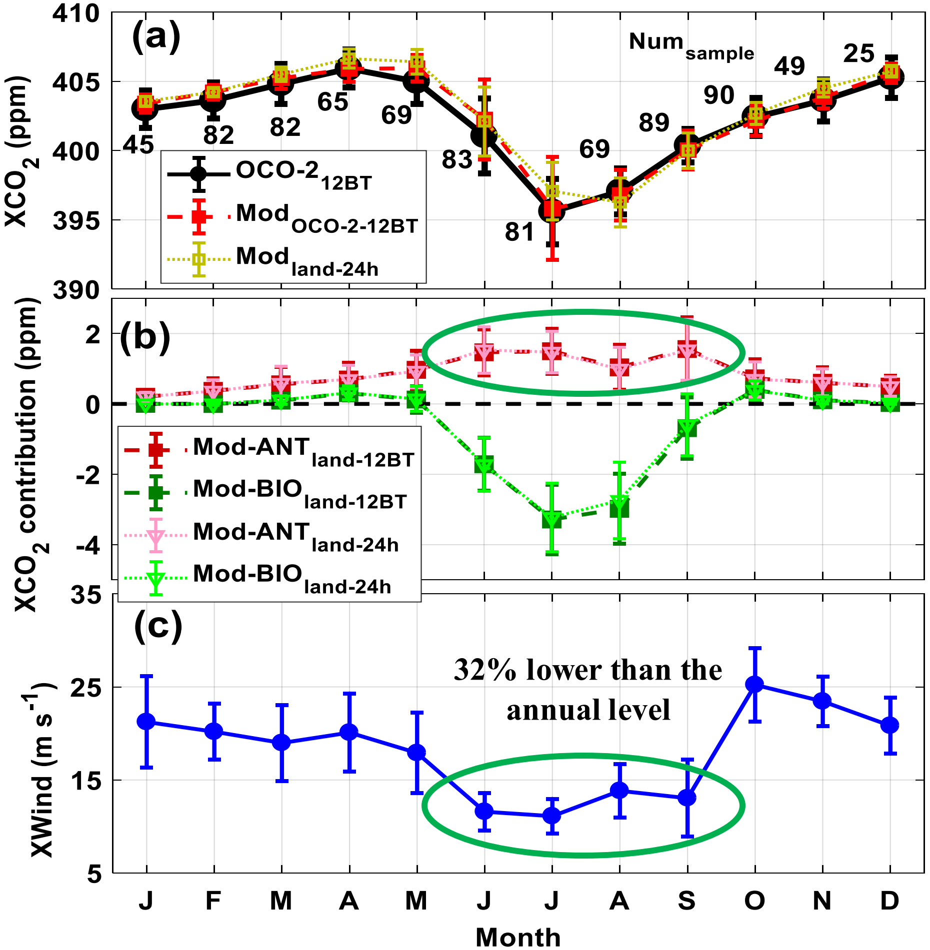


Seasonal variation range: 10 ppmv

**Annual mean contribution:**

- anthropogenic: 0.84 ppmv
- biogenic: -0.60 ppmv

Weak winds favors the large anthropogenic contribution of $XCO_2$ in summer

# Mean diurnal variation of $CO_2$ fluxes and concentrations in growing season

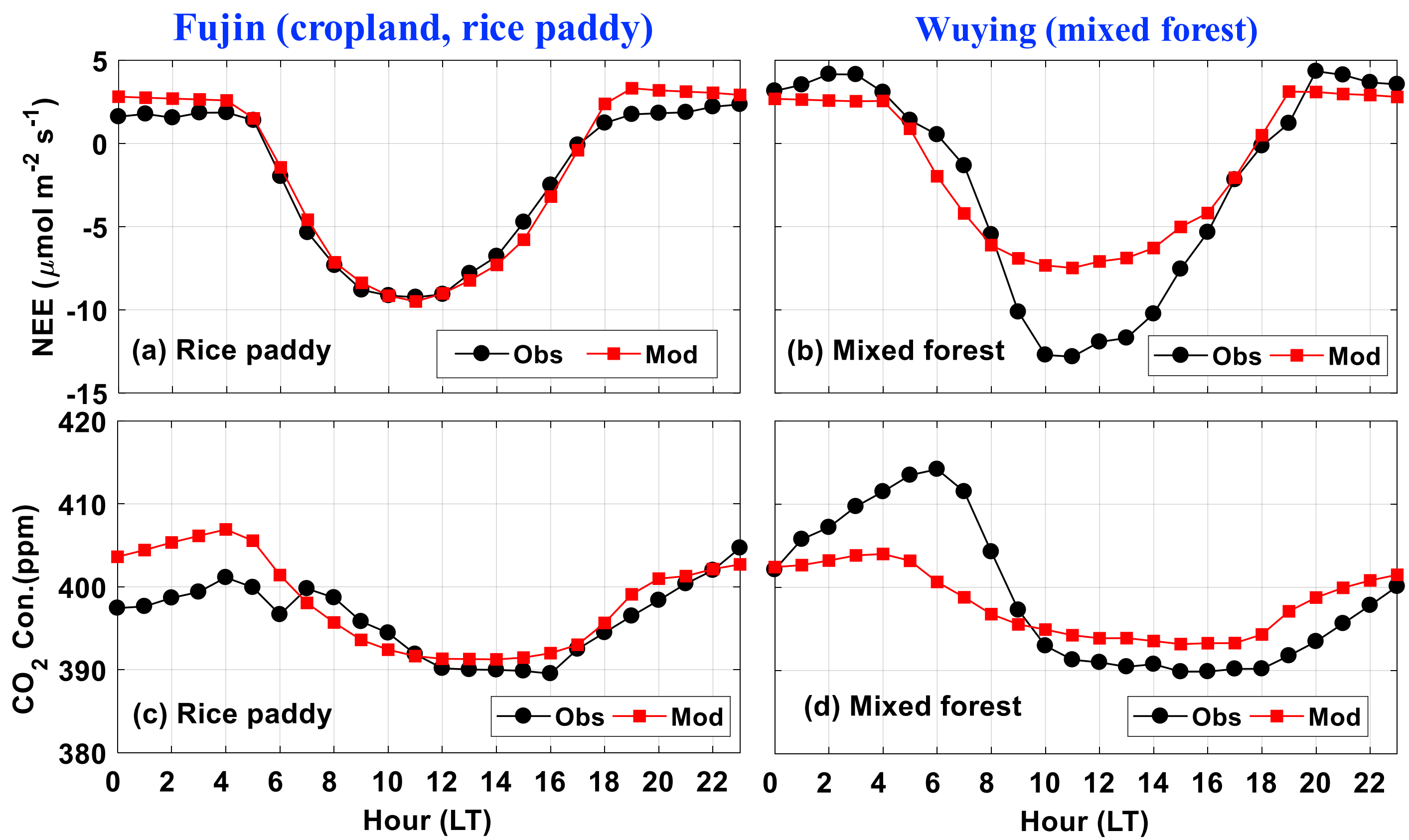


WRF-VPRM underestimates diurnal variation range over mixed forest

# Conclusions and future work

- **Mixed forest is observed as a stronger $CO_2$ sink/source than rice paddy on average in 2016;**
- **Negative biogenic contribution offset about 70% of anthropogenic contribution of $XCO_2$ over Northeast China in 2016;**
- **The uncertainty of NEE simulation largely depends on four VPRM parameters, especially the maximum light use efficiency $\lambda$.**

# Further improvement of WRF-VPRM
# Updated $CO_2$ flux parameterization

$$\mathrm{ER} = \alpha \times T + \beta$$

(Gourdji et al., 2020):

$$ER = \beta + \alpha_1 \cdot T + \alpha_2 \cdot T^2 + \gamma \cdot EVI + k_1 \cdot W_{scale} + k_2 \cdot W_{scale} \cdot T + k_3 \cdot W_{scale} \cdot T^2$$

incorporating EVI, water stress scaling factor ($W_{scale}$), and a quadratic dependence on Tair

More details in Hu et al., 2021, JGR

# $CO_2$ flux evaluation

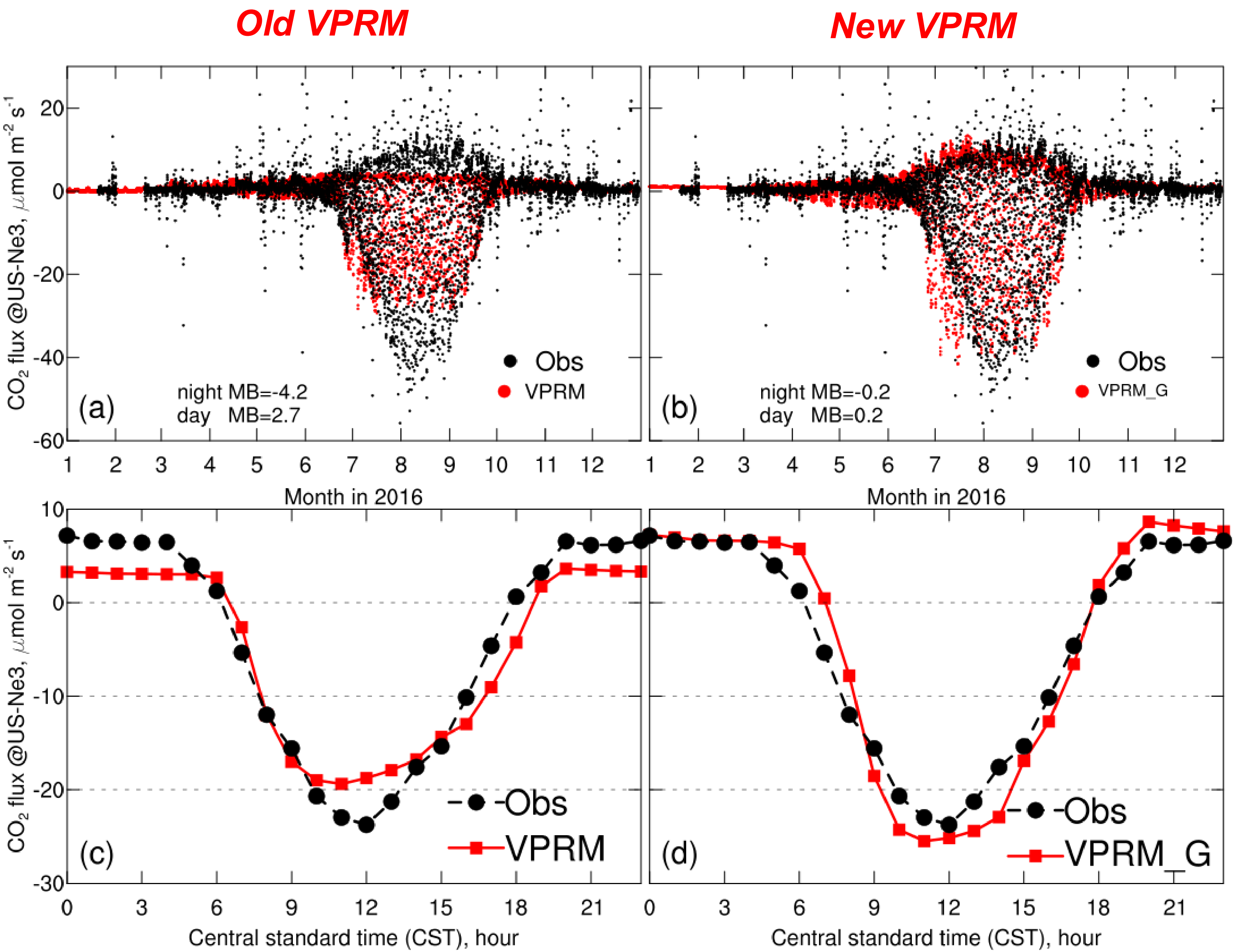

# Evaluation data: NOAA towers

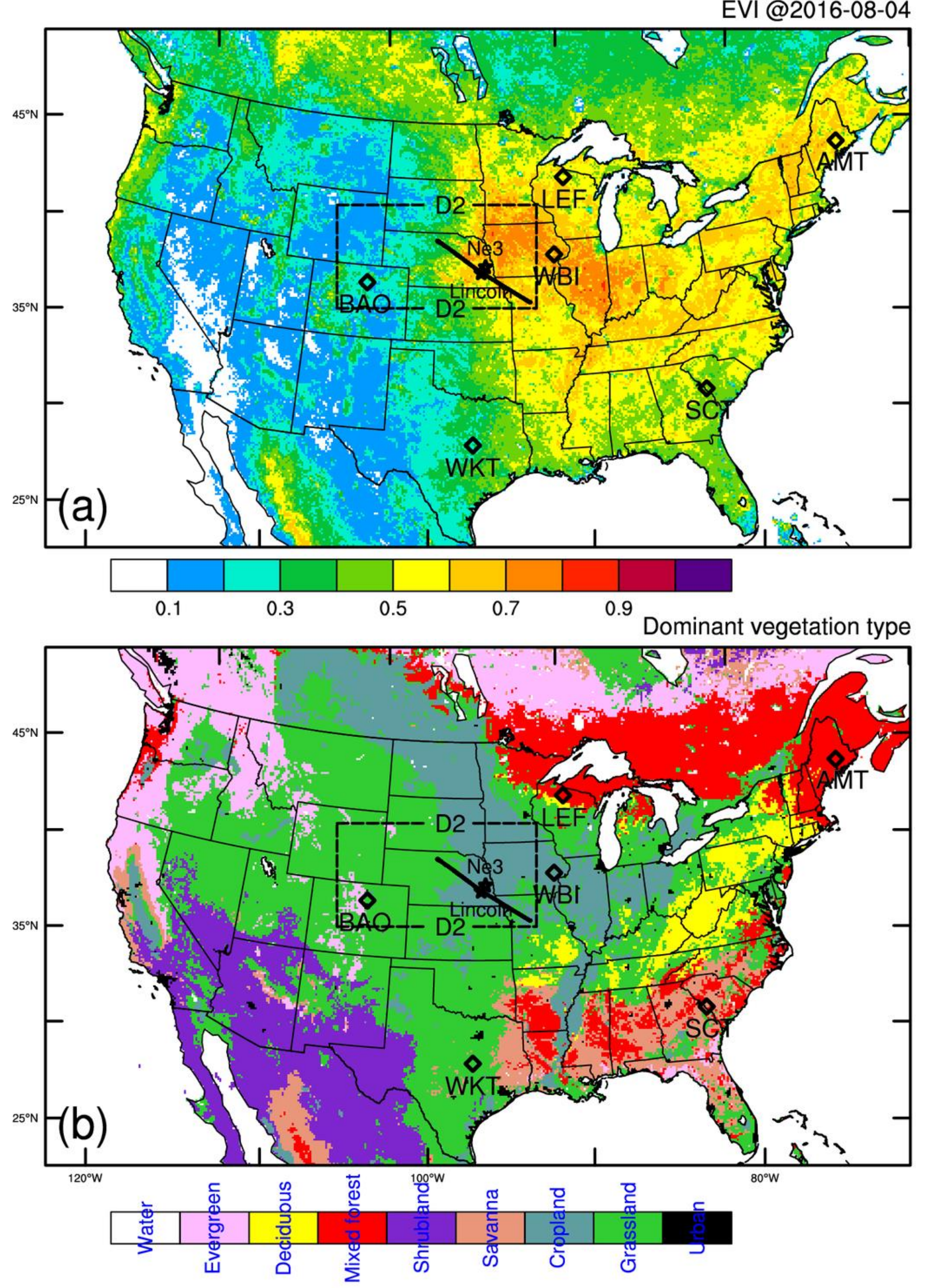

# $CO_2$ concentration evaluation

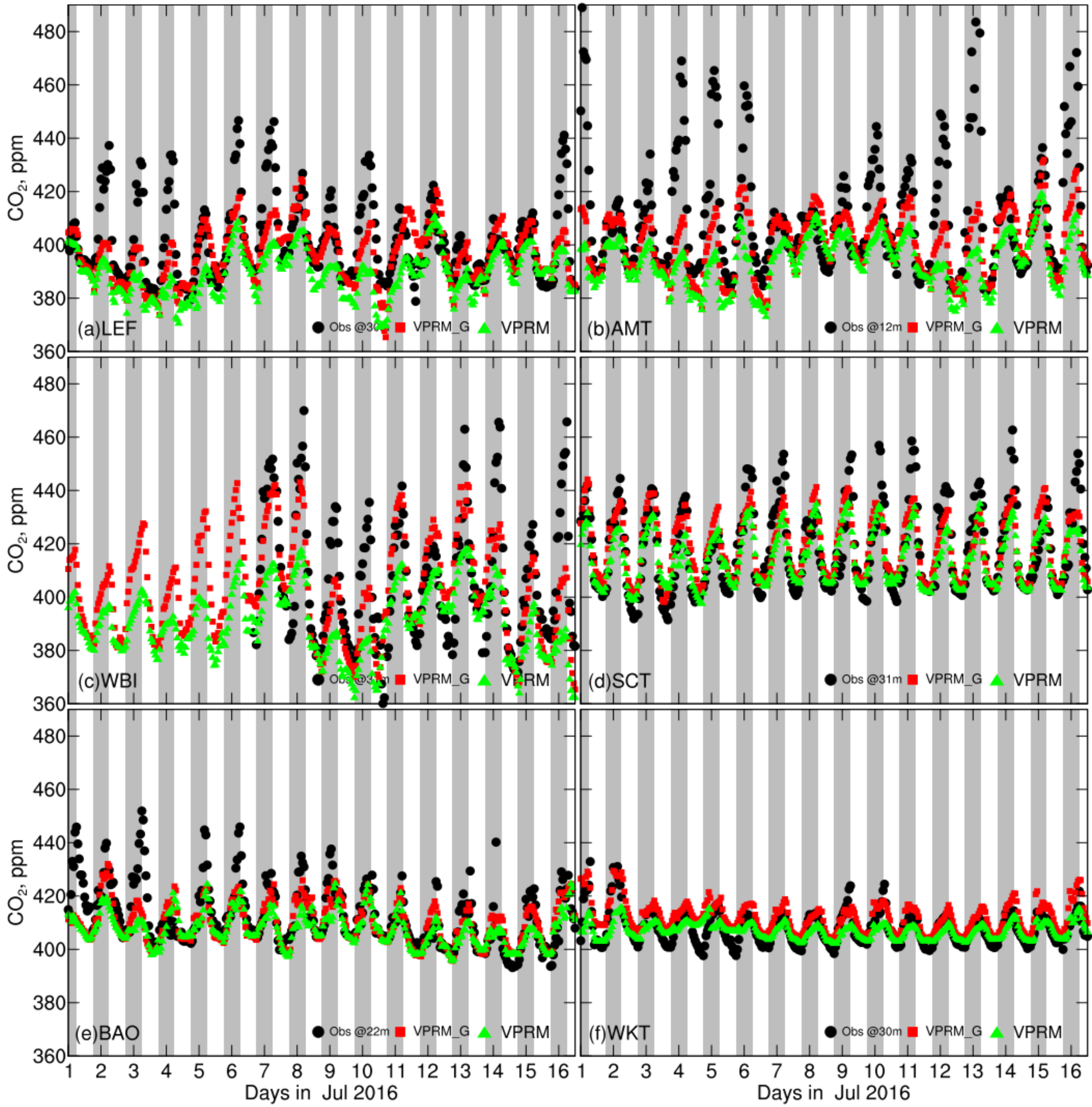

# Using new VPRM to examine $CO_2$ band

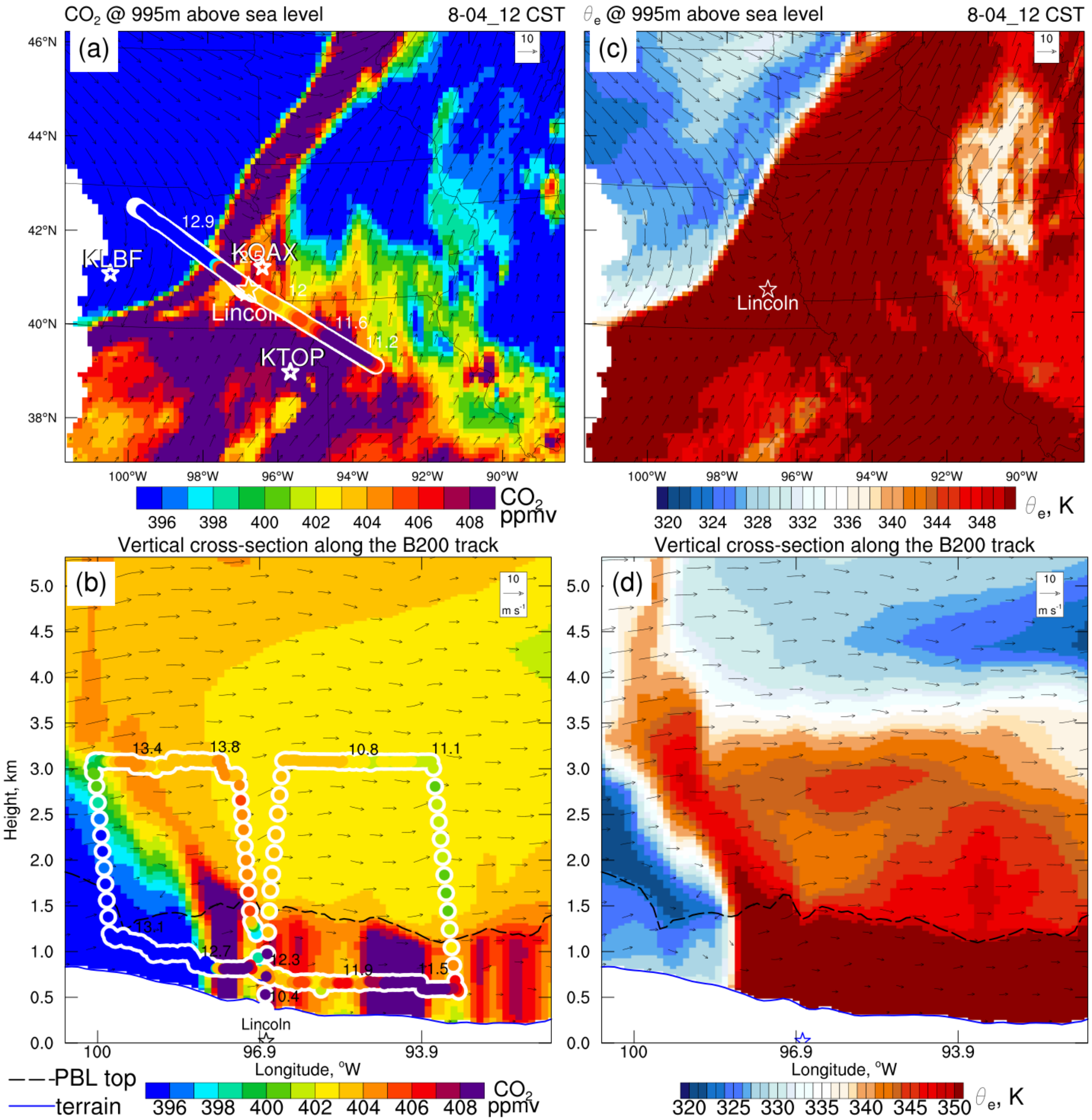

# Application of improved WRF-VPRM in China to examine $CO_2$ flux

| Name | Site | Altitude (m) | Substrate |
|---|---|---|---|
| Maqu | 33.8975° N, 102.1619° E | 3423 | Kobresia tibetica and K. humilis |
| Yakou | 38.0142° N, 100.2421° E | 4148 | Alpine grassland |
| Dashalong | 38.8399° N, 98.9406° E | 3739 | Swampy alpine meadows |
| Arou | 38.0473° N, 100.4643° E | 3033 | Alpine grassland |
| Nam CO | 30.7667° N, 90.95° E | 4730 | K. pygmaea and alpine steppe |
| Mt. Waliguan | 36.28° N, 100.9° E | 3810 | Arid and semi-arid grasslands, tundra, and deserts |

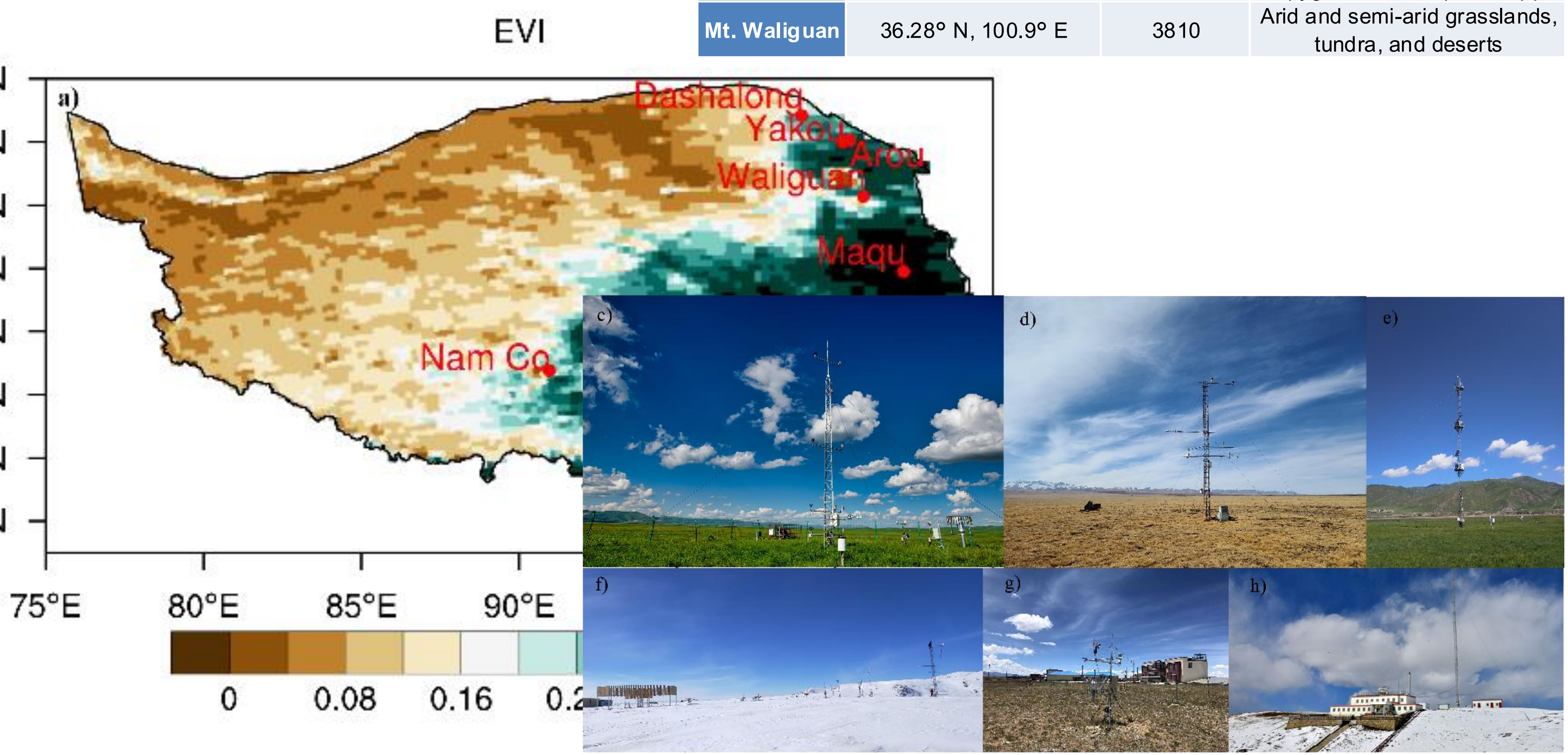


Niu and Hu et al. (2023)

# Application of improved WRF-VPRM in China to examine $CO_2$ flux

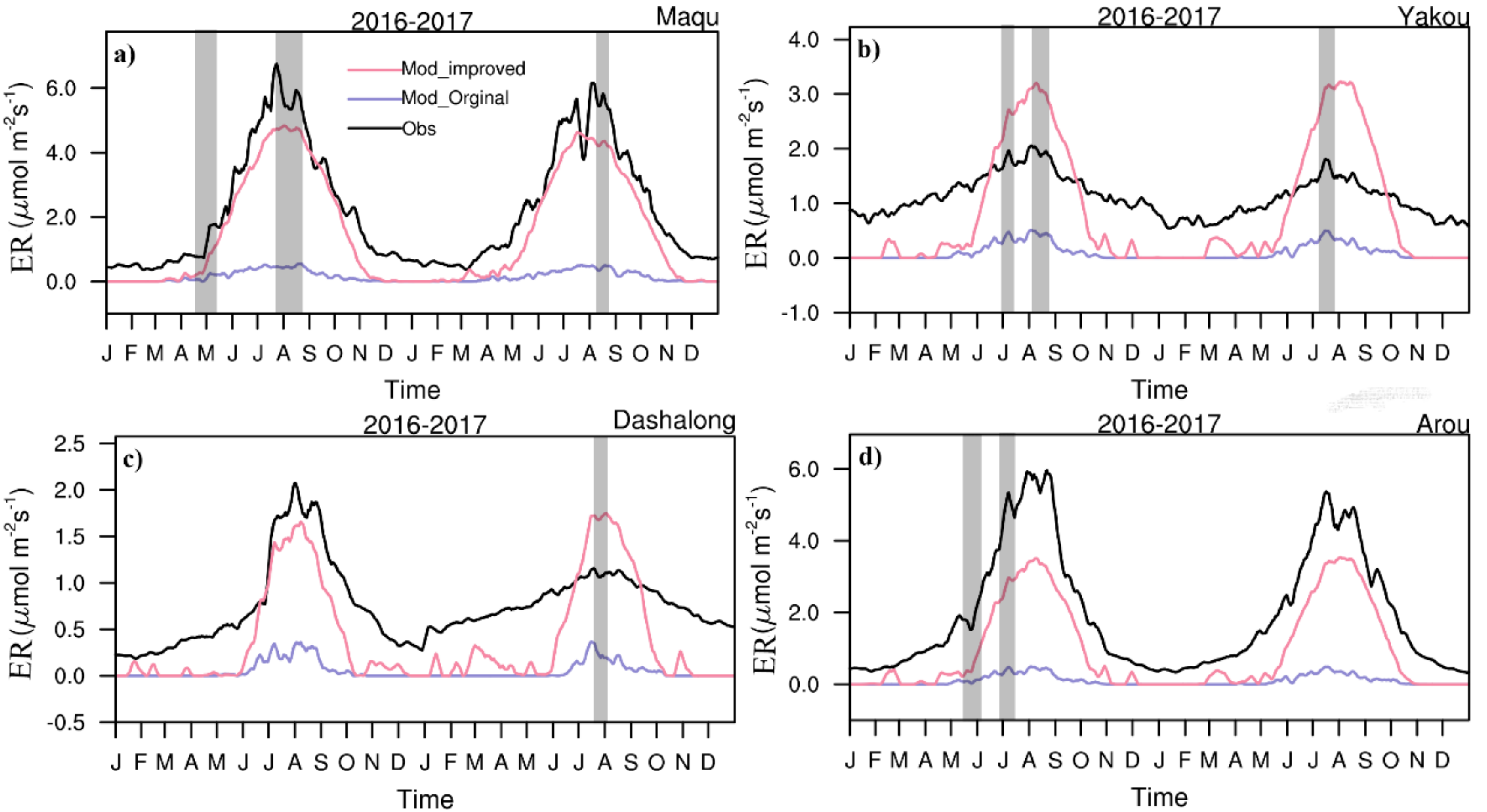


Niu and Hu et al. (2023)

# Application of improved WRF-VPRM in China to examine $CO_2$ flux

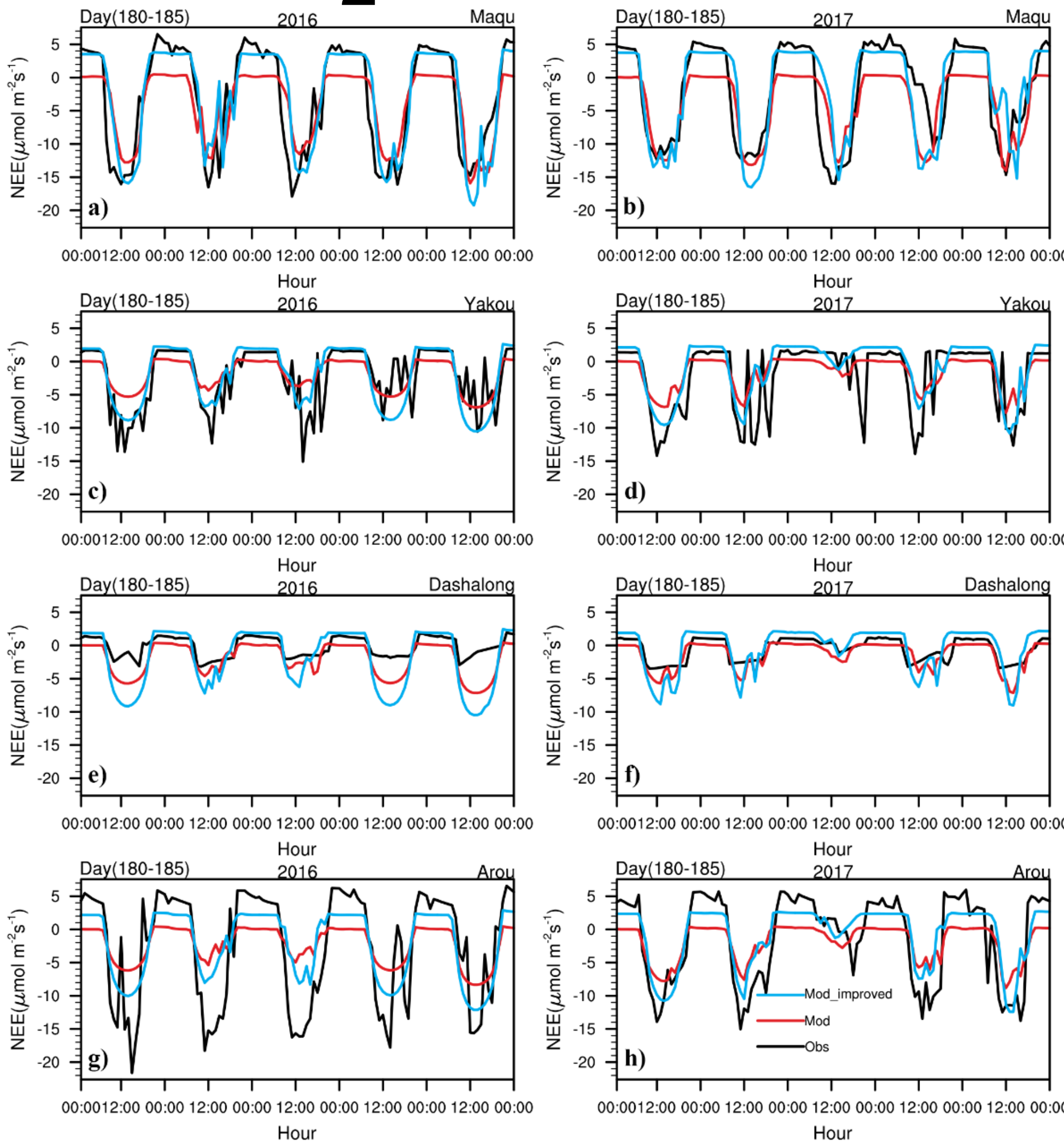


Niu and Hu et al. (2023)

**1. 3D WRF-CO2 simulation**

Over US and China

**2. Multi-Model investigation of Haze Pollution**

**3. WRF-GHG for both $CO_2$ and $CH_4$ simulation**

**4. CH4 inversion**

# Haze pollution in China

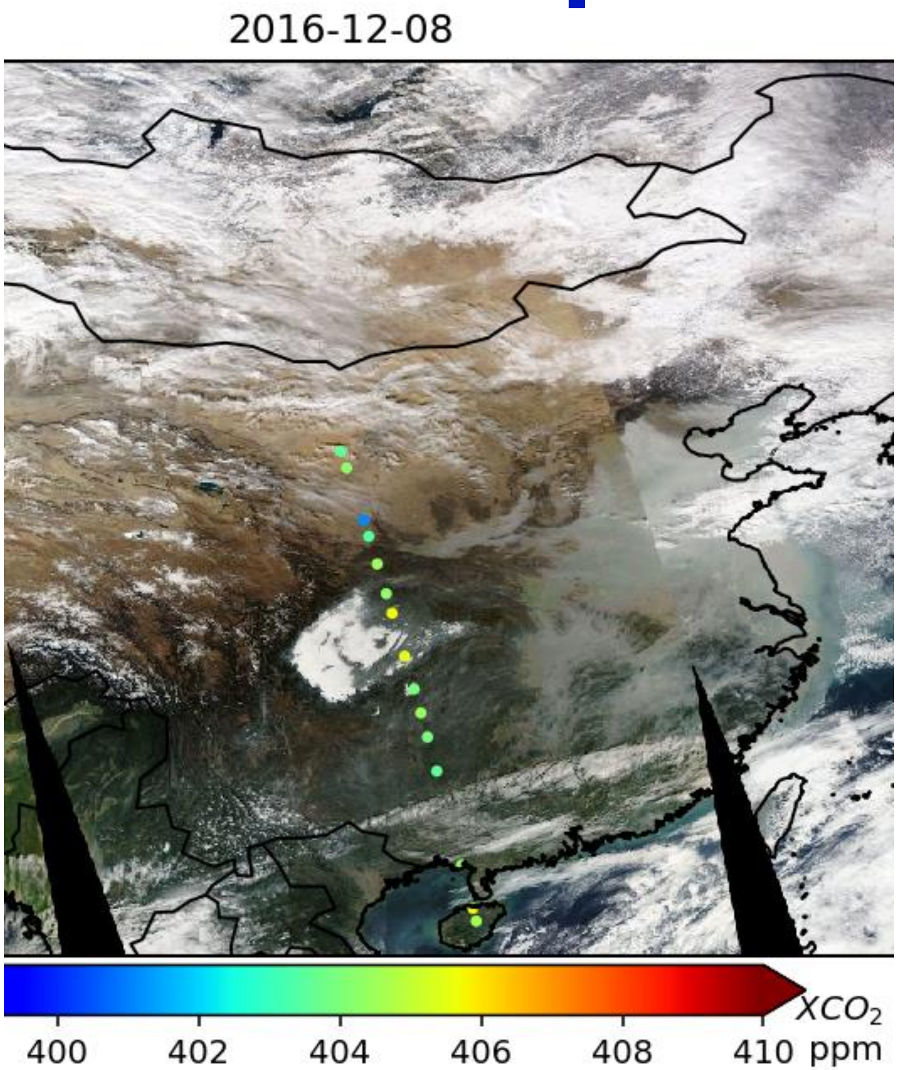


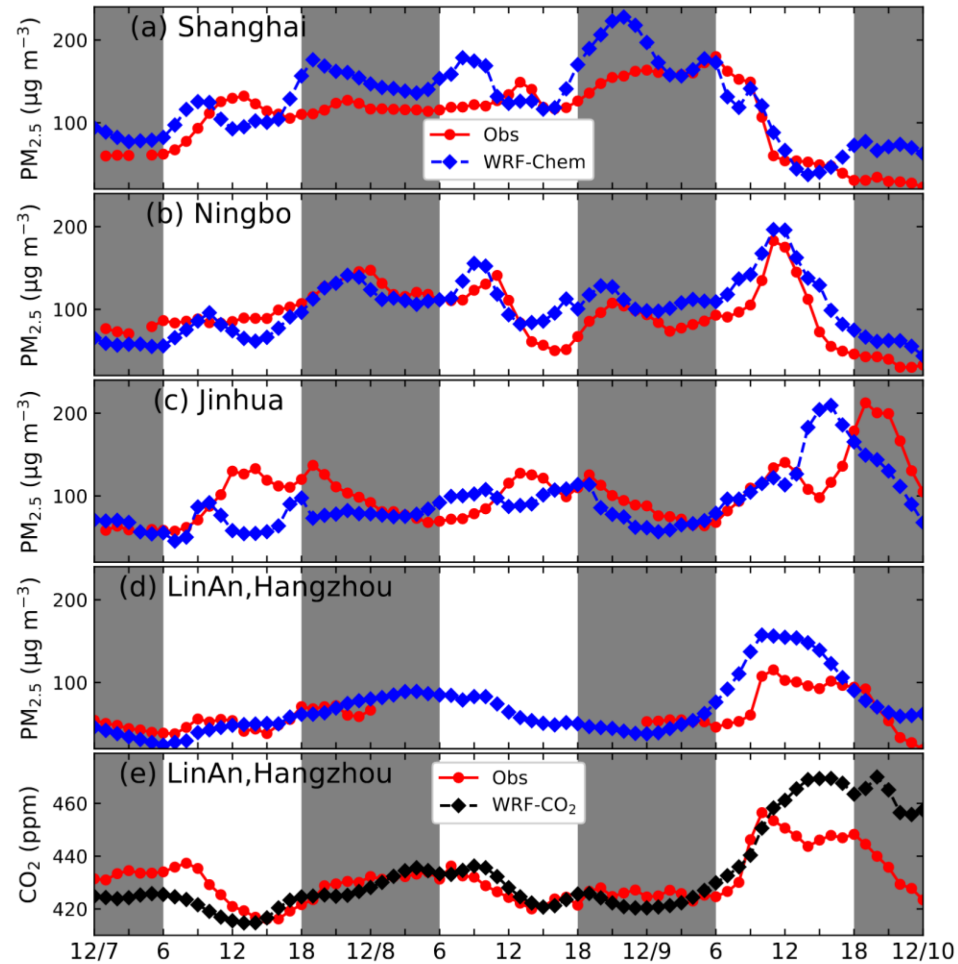


*Heaviest haze pollution in China in 2016*

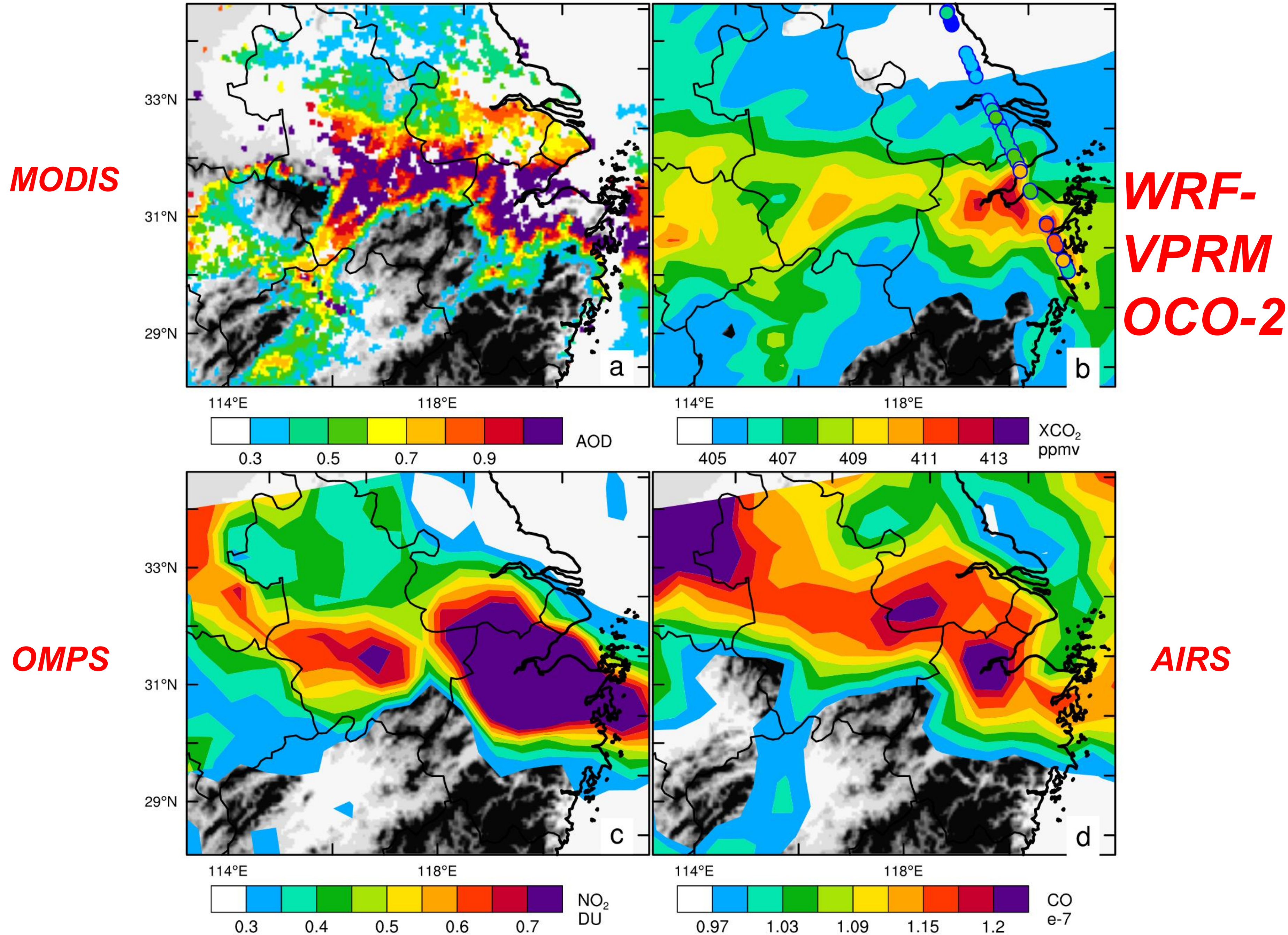
MODIS
WRF-
VPRM
OCO-2
OMPS
AIRS
33°N
31°N
29°N
114°E
118°E
a
b
c
d
AOD
0.3
0.5
0.7
0.9
XCO2
ppmv
405
407
409
411
413
NO2
DU
0.3
0.4
0.5
0.6
0.7
CO
e-7
0.97
1.03
1.09
1.15
1.2

# Conclusions

1. **A severe haze pollution at the leading edge of a cold front in China on Dec. 9, 2016 is examined using multi-sensors and multi-models, including WRF-Chem and WRF-$CO_2$.**

2. **Satellite-retrieved column-averaged $CO_2$ data can be used to monitor air pollution events collectively with other in situ and remote-sensing instruments.**

3. **Channel winds between Mountains Dabie and Huang transport pollutants from the North China Plain and Yangtze River Delta Region to Jiangxi Province**

**1. 3D WRF-CO2 simulation**

Over US and China

**2. Multi-Model investigation of Haze Pollution**

**3. WRF-GHG for both $CO_2$ and $CH_4$ simulation**

**4. CH4 inversion**

# WRF-GHG coupled with CAMS

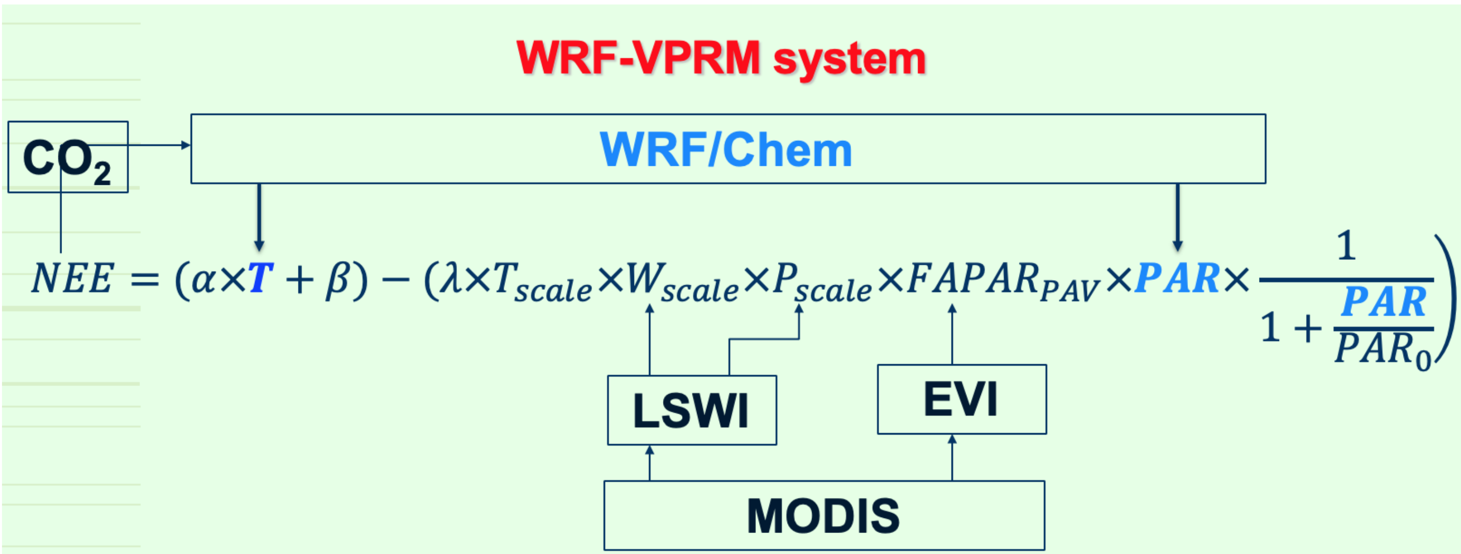


Included $CH_4$ recently doi/10.1002/essoar.10508159.1

the *WetCHARTs* wetland $CH_4$ emissions

EPA NEI2017 anthropogenic $CH_4$ emissions

# WRF-GHG simulation vs. TCCON observation

$CO_2$

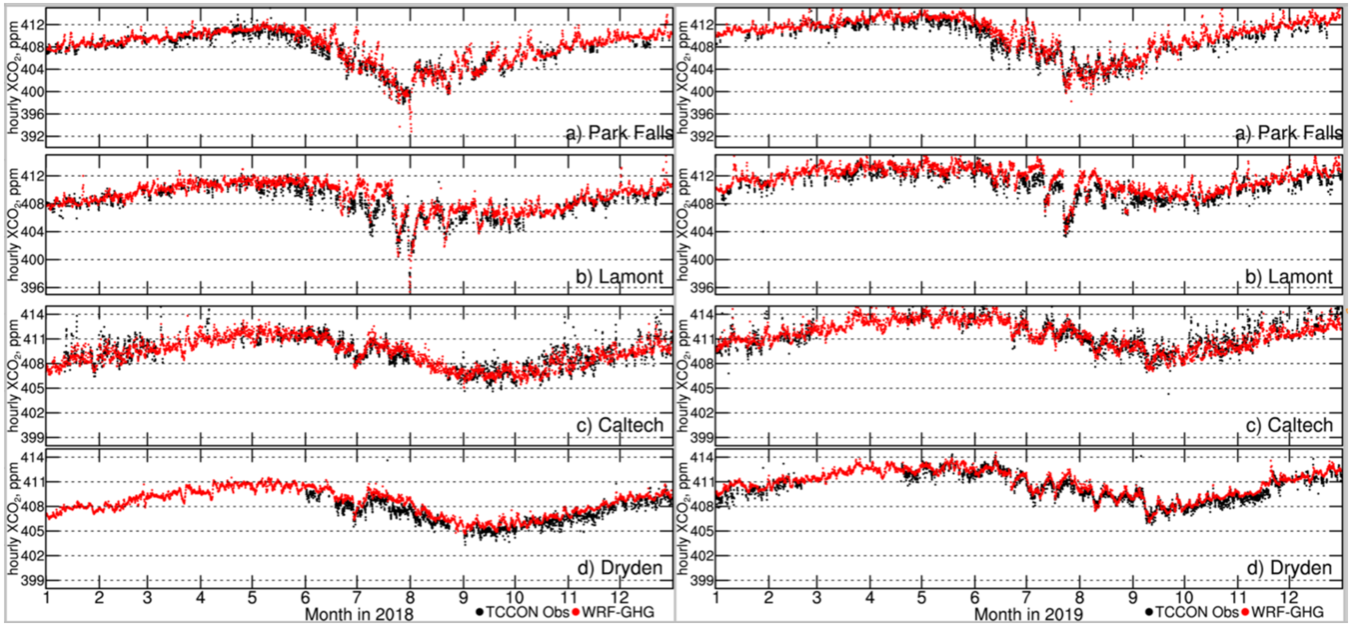


$CH_4$

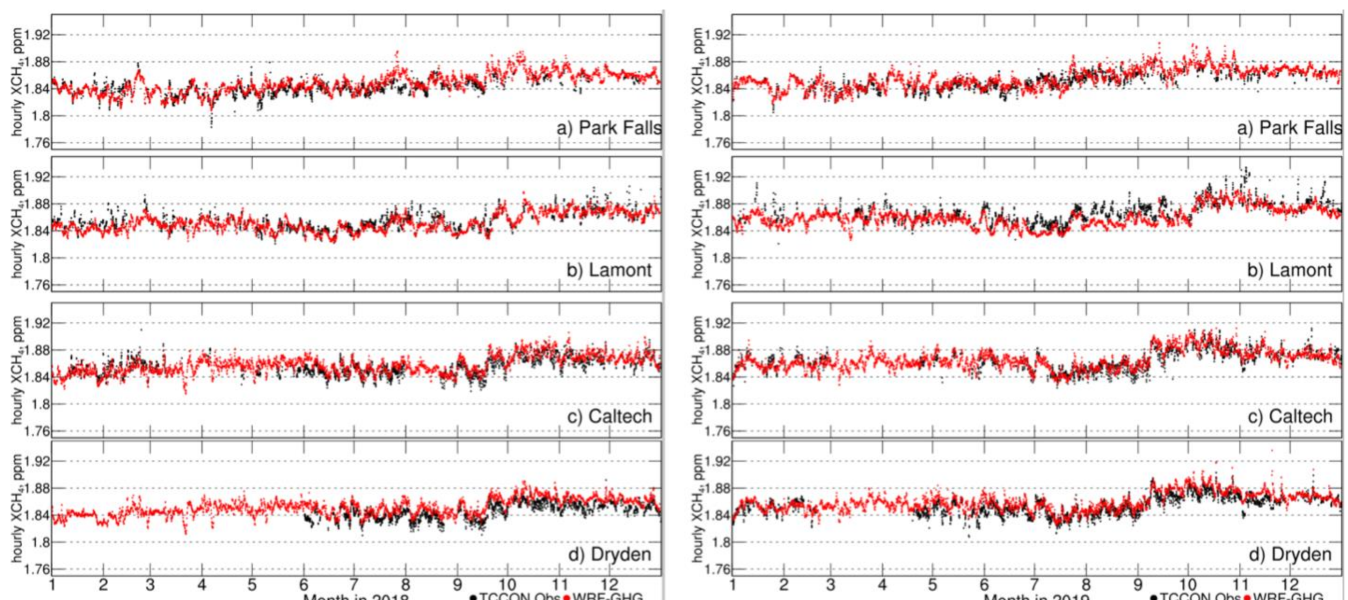

# Difference of EVI between 2018 and 2019

***June***

**EVI_diff 2019-2018 06-26_18:00:00**

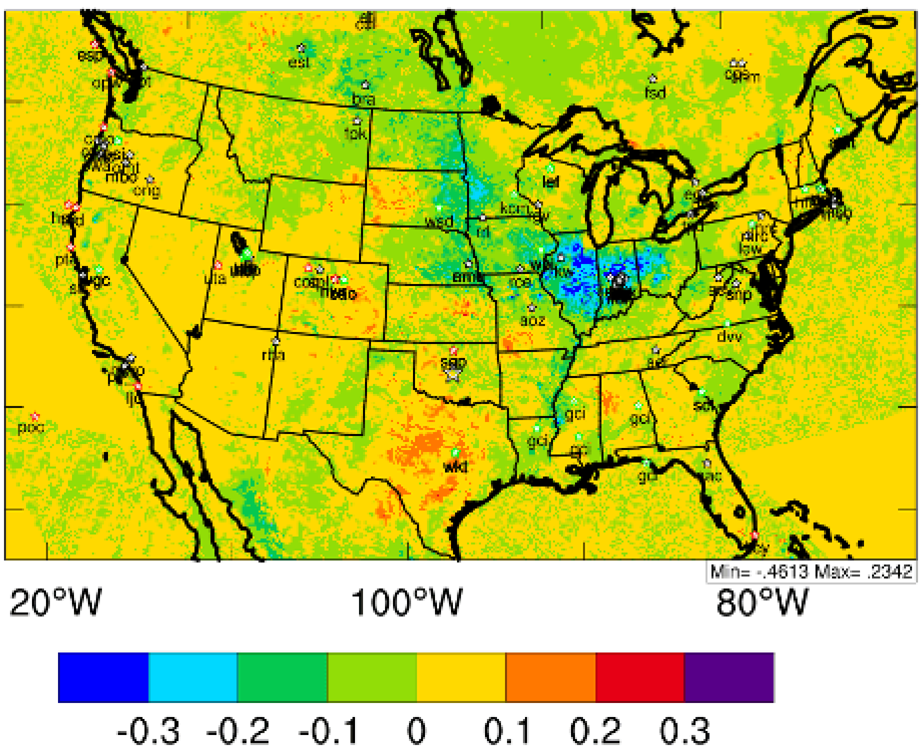


***Sept***

**EVI_diff 2019-2018 09-21_18:00:00**

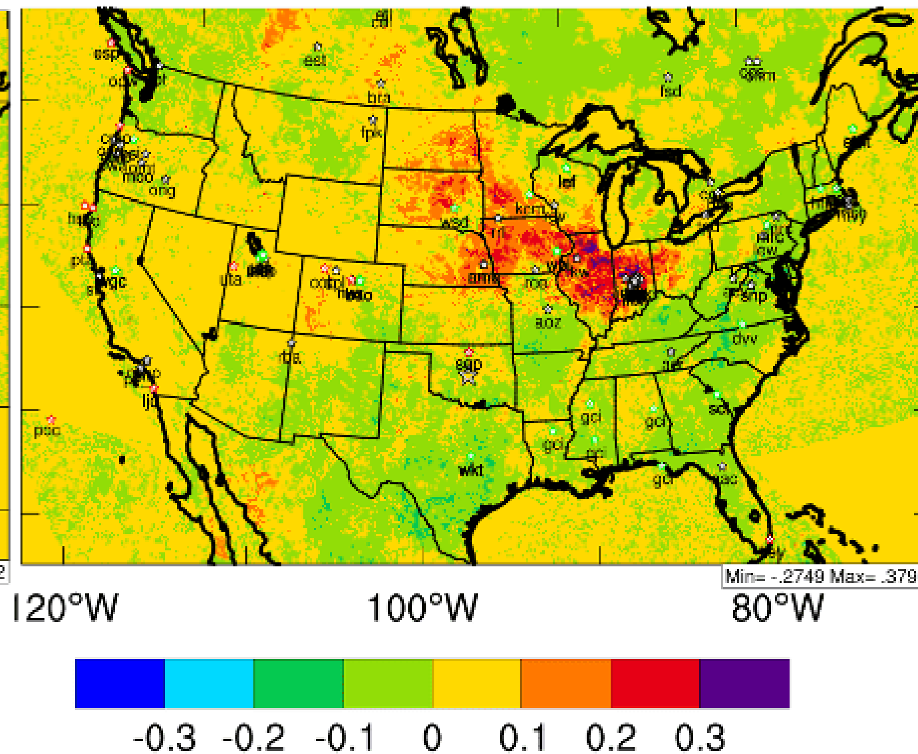


Flood delayed growing season

# 2019 flood delayed the drawdown of $CO_2$ in summer

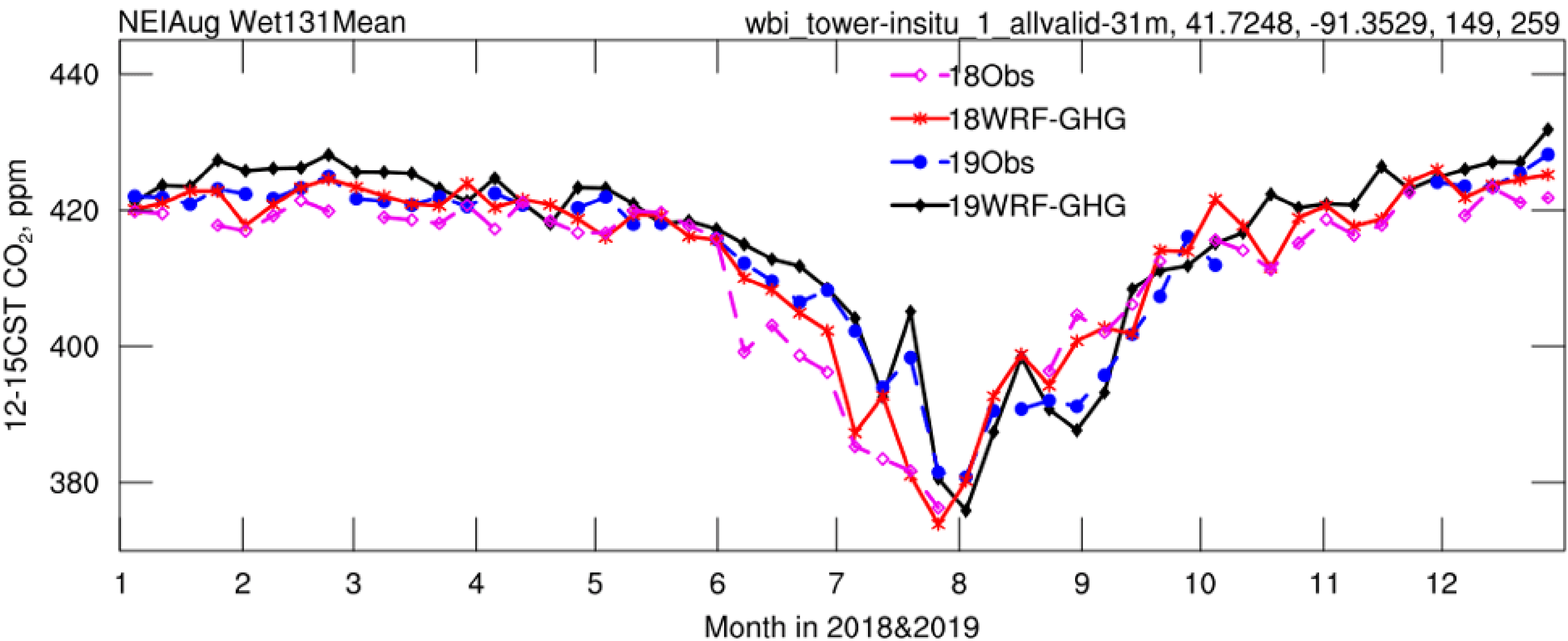

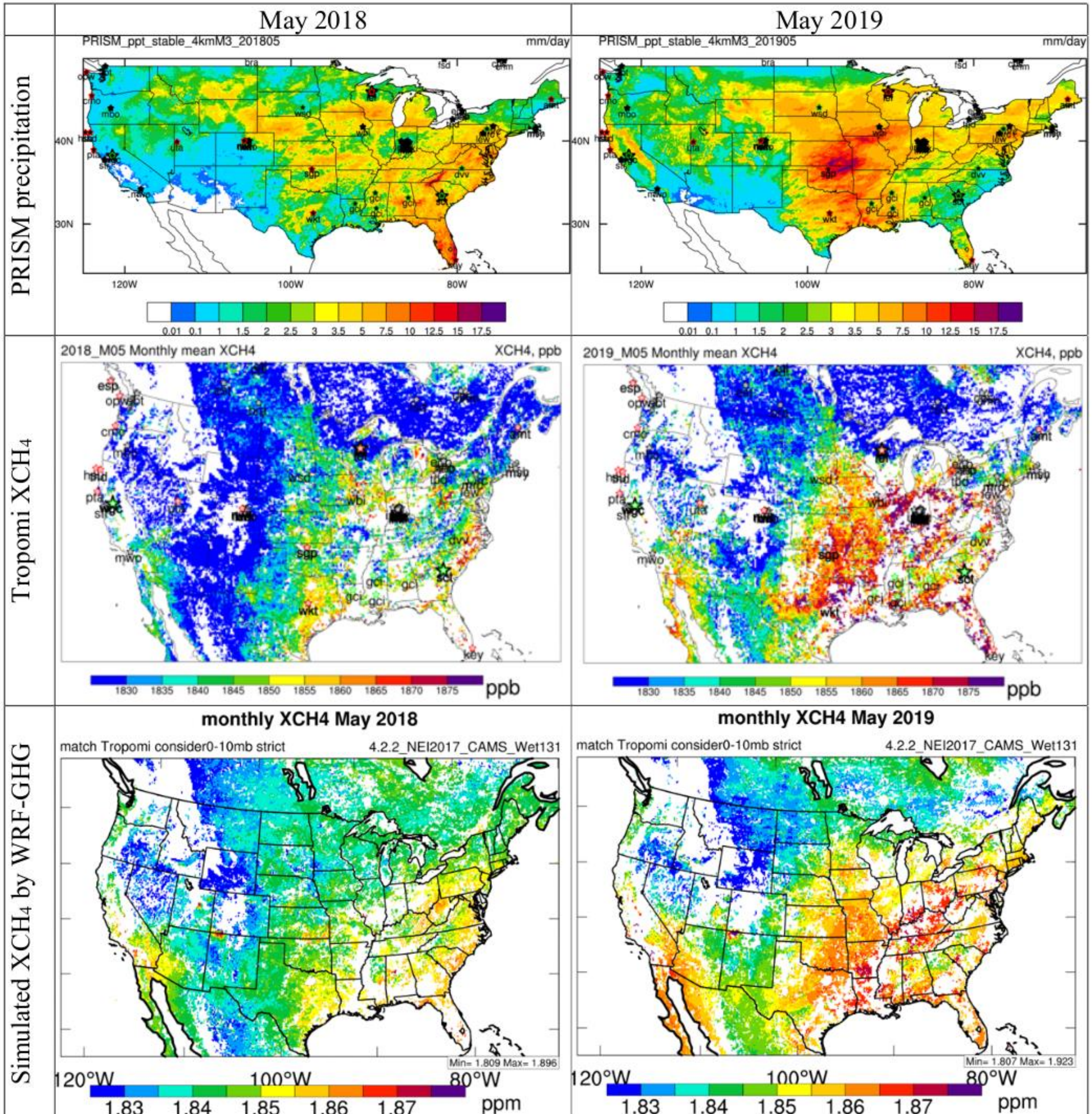
May 2018
May 2019
PRISM precipitation
PRISM_ppt_stable_4kmM3_201805
mm/day
PRISM_ppt_stable_4kmM3_201905
mm/day
40N
30N
120W
100W
80W
0.01 0.1 1 1.5 2 2.5 3 3.5 5 7.5 10 12.5 15 17.5
Tropomi XCH4
2018_M05 Monthly mean XCH4
XCH4, ppb
2019_M05 Monthly mean XCH4
XCH4, ppb
1830 1835 1840 1845 1850 1855 1860 1865 1870 1875
ppb
Simulated XCH4 by WRF-GHG
monthly XCH4 May 2018
monthly XCH4 May 2019
match Tropomi consider0-10mb strict
4.2.2_NEI2017_CAMS_Wet131
Min= 1.809 Max= 1.896
Min= 1.807 Max= 1.923
120°W
100°W
80°W
1.83 1.84 1.85 1.86 1.87
ppm

# $CH_4$ bias against Obspack due to precipitation bias?

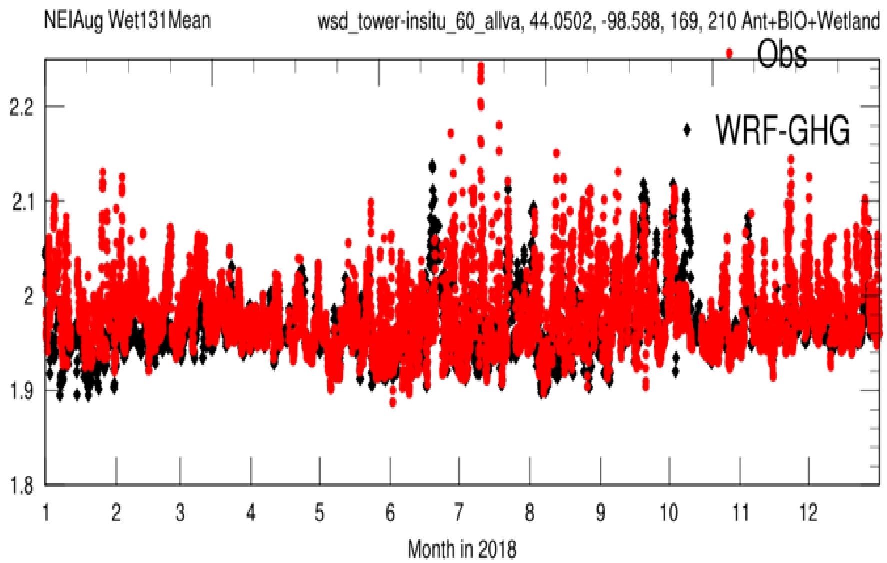


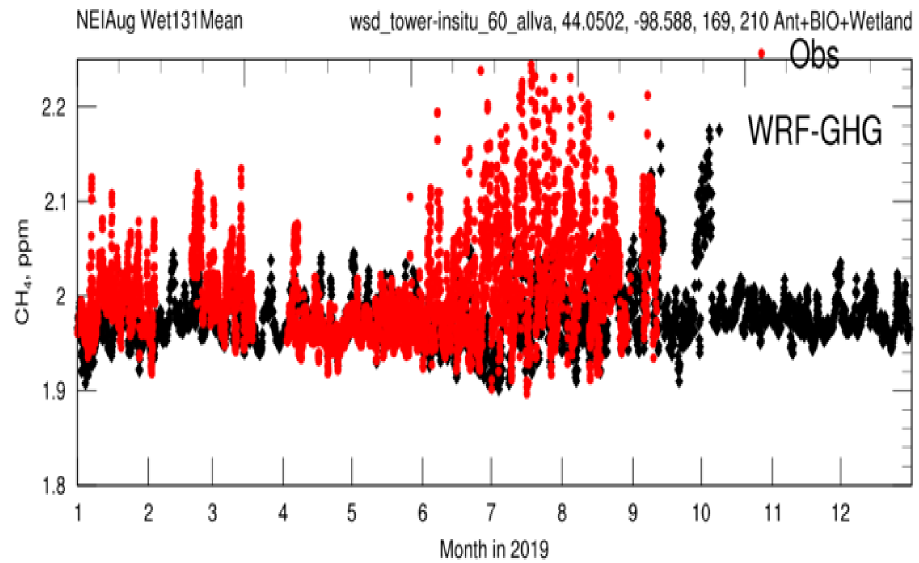


Waiting for PRISM-driven WetCharts $CH_4$ emission

# Summary

1. WRF-GHG is further developed to simulate $CO_2$ and $CH_4$.
2. The 2019 May flood delayed growing season in mid-west and the typical spring and summer drawdown of atmospheric $CO_2$ by 1-3 weeks
3. Obspack and TROPOMI data indicate higher $CH_4$ in the mid-west in July and August, in 2019 relative to 2018, due to the abnormal precipitation in 2019 in the region that induces more wetland $CH_4$ emissions.

**1. 3D WRF-CO2 simulation**

Over US and China

**2. Multi-Model investigation of Haze Pollution**

**3. WRF-GHG for both CO2 and CH4 simulation**

**4. CH4 inversion**

# Table 1, Summary of advantages and disadvantages of different top-down flux quantification techniques

| Category | Method | Description | Strengths | Limitations | References |
|---|---|---|---|---|---|
| Mass Conservation Based | Local Mass Balance | Estimates $CH_4$ emissions by integrating the concentration across a defined plane downwind of the source. | Simple to implement; useful for local or regional flux estimation | Highly dependent on accurate wind speed and direction; Often need aircraft campaign to collect vertical $CH_4$ profile | Cambaliza et al. (2014); Johnson and Johnson (1995); Spokas et al. (2006) |
| | Gauss's Theorem Method | The outward flux summed along a contour surrounding the point source | Closed circle, good for single or contained sources | Highly dependent on accurate wind speed and direction; also need $CH_4$ concentration observations | Conley, Faloona et al. (2017), Ryoo, Iraci et al. (2019) |
| | Integrated Mass Enhancement | Based on satellite observations: The total mass enhancement in the plume is related to the magnitude of emission with a parameterization dependent on wind speed. | Useful for large-scale emissions detection and satellite data utilization | Relies on assumptions about atmospheric mixing and wind patterns; cannot resolve small-scale or intermittent emissions | Bhardwaj, Kumar et al. (2022) |
| | Angular Width | Based on satellite observations: Infer source rates without independent wind information by using the plume angular width as a measure of wind speed. | Provides an alternative to wind-measurement-dependent models; useful when meteorological data is limited | Assumes uniform plume dispersion; sensitive to plume geometry and wind patterns | Jongaramrungruang, Frankenberg et al. (2019) |
| | Tracer Correlation Method | Releasing known quantities of tracer gas(es), e.g., $N_2O$ close to a suspected source, the unknown methane flow was deduced based on the known tracer flow and the measured concentration enhancements | Doesn't require detailed atmospheric dispersion modeling; can be deployed in varied environments | Requires separate tracer gas release, which can be logistically difficult | Galle, Samuelsson et al. (2001), Sisterson, Peppler et al. (2016) |
| Gaussian Dispersion Based | Gaussian Plume Model | Assumes the $CH_4$ concentration emitted from a point source follows a Gaussian distribution in space. | Well-suited for point-source emissions; simple and easy to use | Highly dependent on accurate wind speed and direction; also need $CH_4$ concentration observations | Grauer et al. (2018); Matacchiera et al. (2019); Varon et al. (2018) |
| Lagrangian Particle Dispersion Based | Lagrangian Stochastic Particle Dispersion Model | Simulates the transport and dispersion of $CH_4$ using particle trajectories in the atmosphere. | More accurate than Gaussian models in complex environments; accounts for surface roughness and non-uniform meteorological conditions | Highly dependent on accurate meteorological inputs | Gao et al. (2008); Gao et al. (2009); Laubach and Kelliher (2005) |
| Data assimilation methods Bayesian Theory Based | Ensemble Kalman Filter (EnKF) | Assimilates $CH_4$ observational data to iteratively update model states, using an ensemble forecast. | Dynamically accounts for uncertainties in model states and measurements; handles time-dependent variations | Computationally demanding; requires a high-quality ensemble of meteorological inputs | Bisht et al. (2023); Platonova and Klimova (2021) |
| | Variational Method (4DVar) | the model's posterior over time is adjusted to minimize the discrepancies between the model output and observations of methane emissions over a time window. | Allows for dynamic error evolution, providing detailed spatiotemporal corrections of methane fluxes. | Computationally expensive and requires an adjoint model, which can be difficult to develop. | Wilson, Chipperfield et al. (2014), Bannister and Wilson (2024) |
| | Markov Chain Monte Carlo | It samples from the posterior distribution of model parameters or state variables, providing a probabilistic estimate by generating a large number of samples. | Provides a thorough exploration of parameter space; useful for uncertainty quantification in methane emissions estimation | Can be slow to converge; computationally demanding | Western, Ramsden et al. (2021) |
| | Other Bayesian inference Based Methods | Bayesian inference techniques estimate $CH_4$ emissions by iteratively updating a prior emission estimate using observational data and optimizing the posterior distribution of the emission. | Uses probabilistic framework; effectively incorporates uncertainties in the model and data, handles non-linear dynamics well | Computationally expensive; sensitive to prior assumptions, and convergence can be slow depending on the complexity of the model | Thompson, Sasakawa et al. (2017), Cusworth, Bloom et al. (2021) |
| Machine Learning Based | Convolutional Neural Network | Machine learning-based approach that learns from observed methane concentrations to estimate emission sources by identifying spatial patterns. | Highly adaptable to large datasets; can discover complex, non-linear relationships between emissions and observed concentrations | Requires large amounts of data to train; susceptible to overfitting, and can be difficult to interpret | Jahan, Mehana et al. (2024) |
| | Random Forests | Machine learning approach that aggregates decision trees to predict methane emissions based on various input variables, such as meteorological conditions and observed concentrations. | Handles complex interactions between variables well; robust against overfitting with appropriate tuning | Requires careful feature selection; may not generalize well beyond training data | Irvin, Zhou et al. (2021), Räsänen, Manninen et al. (2021) |

## Table 1, Summary of advantages and disadvantages of different top-down flux quantification techniques

| flux quantification techniques | | Advantages | disadvantages |
|---|---|---|---|
| Conventional simple methods | Mass balance box methods | Simply quantify the emissions using the total flux out of the box covering the emission sources | Require dense spatial sampling or interpolation/extrapolation |
| | Gaussian plume inversion | Simply quantify the emissions using the Gaussian plume equation | Assume Gaussian distributed plume, which is often not valid in conditions with variable winds and large-scale turbulence |
| More advanced methods using three-dimensional simulations | Particle dispersion model inversion (also referred to as scaling factor method) | Calculate the emission using the emission-concentration relationship calculated by the dispersion model, good for a single point source | Only scale the pre-assumed emissions without changing the spatial distribution, cannot attribute to different emission locations |
| More advanced methods through data assimilation | 4D-Variational (4D-Var) approach | 4D-Var is computationally efficient due to no requirement of ensemble forecast<br>4D-Var performs well over data sparse regions | Require abjoint model development |
| | Ensemble Kalman Filter (EnKF) | Quantify emission using flow-dependent error covariance between emissions and concentrations derived from short-term ensemble forecasts<br>Meteorological fields can be simultaneously optimized, which leads to better emission estimation | Need re-cycle ensemble forecasts for time-varying emission sources |

# Mass balance methods

$$F = \int_{z_1}^{z_2} \int_{x_1}^{x_2} ([CH_4] - [CH_4]_b) U_\perp \mathrm{d}x\mathrm{d}z,$$

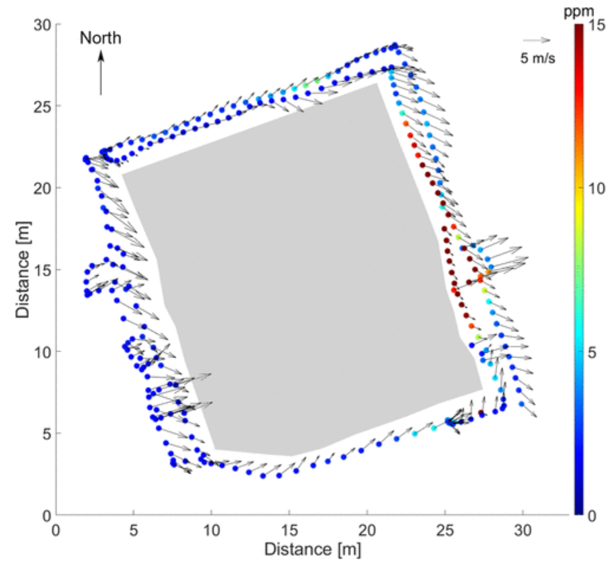


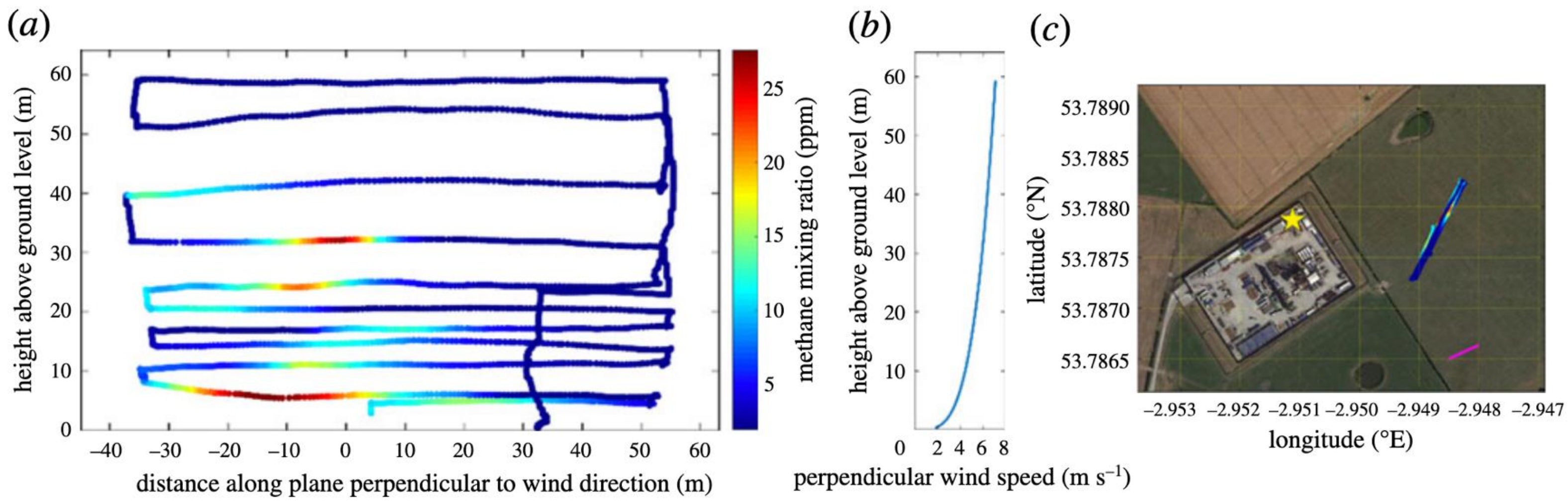

# Gaussian plume inversion

$$[CH_4](y,z) = \left( \frac{F}{2\pi U_{\perp} \sigma_y \sigma_z} \times \exp\left( \frac{-y^2}{2{\sigma_y}^2} \right) \times \left( \exp\left( \frac{-(z-H)^2}{2{\sigma_z}^2} \right) + \exp\left( \frac{-(z+H)^2}{2{\sigma_z}^2} \right) \right) \right) + [CH_4]_{b,}$$

# More advance methods using 3D dispersion models and data assimilation

| flux quantification techniques | | Advantages | disadvantages |
|---|---|---|---|
| Conventional simple methods | Mass balance box methods | Simply quantify the emissions using the total flux out of the box covering the emission sources | Require dense spatial sampling or interpolation/extrapolation |
| | Gaussian plume inversion | Simply quantify the emissions using the Gaussian plume equation | Assume Gaussian distributed plume, which is often not valid in conditions with variable winds and large-scale turbulence |
| More advanced methods using three-dimensional simulations | Particle dispersion model inversion (also referred to as scaling factor method) | Calculate the emission using the emission-concentration relationship calculated by the dispersion model, good for a single point source | Only scale the pre-assumed emissions without changing the spatial distribution, cannot attribute to different emission locations |
| More advanced methods through data assimilation | 4D-Variational (4D-Var) approach | 4D-Var is computationally efficient due to no requirement of ensemble forecast<br>4D-Var performs well over data sparse regions | Require abjoint model development |
| | Ensemble Kalman Filter (EnKF) | Quantify emission using flow-dependent error covariance between emissions and concentrations derived from short-term ensemble forecasts<br>Meteorological fields can be simultaneously optimized, which leads to better emission estimation | Need re-cycle ensemble forecasts for time-varying emission sources |

# Particle dispersion model inversion (also referred to as scaling factor method)

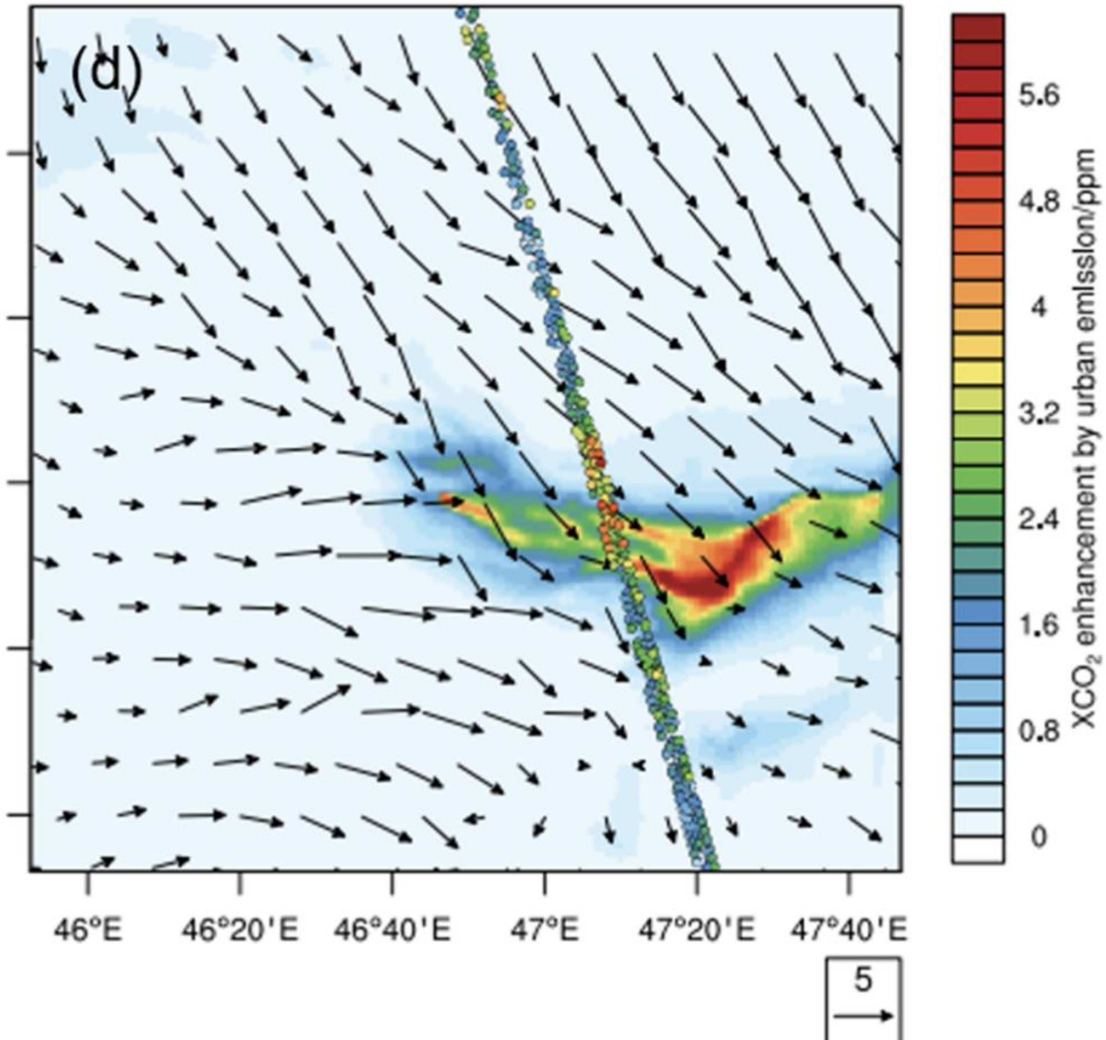

# Data assimilation, 4Dvar vs. EnKF

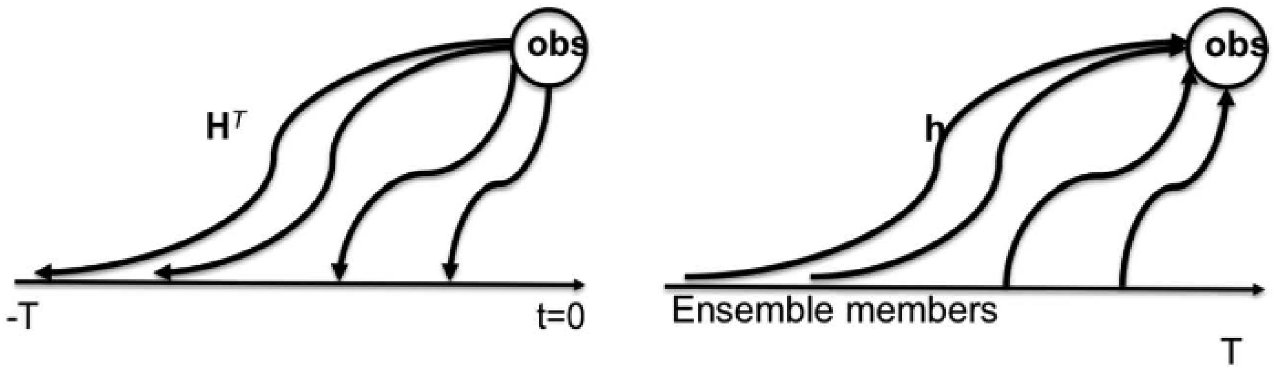


**Figure 1.** Schematic plot showing the differences between (left) 4D-Var and (right) ensemble Kalman filter in calculating the relationship between $CO_2$ concentrations and surface fluxes. $H^T$ is the adjoint of the observation operator including the adjoint of transport model, while $h(\cdot)$ represent the forward observation operator including forward transport model.

Hu et al. 2011, GRL

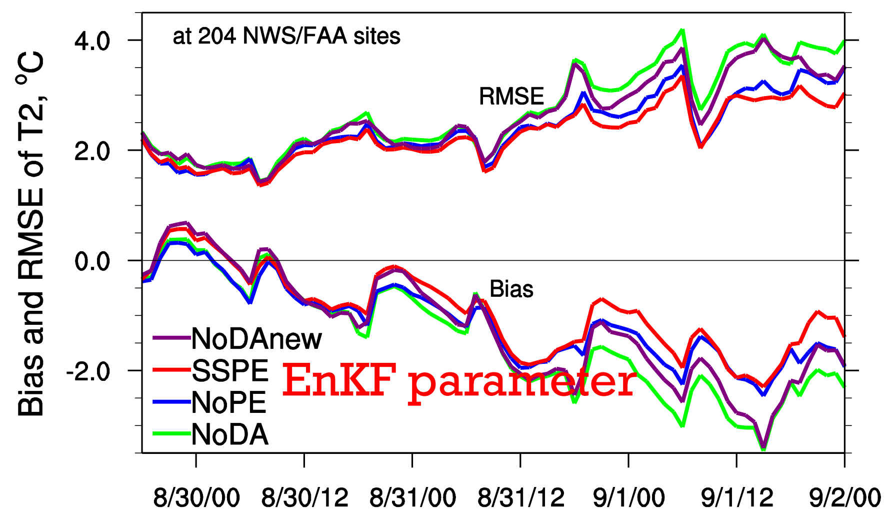

# CH4 flux inversion using EnKF-WRF/GHG

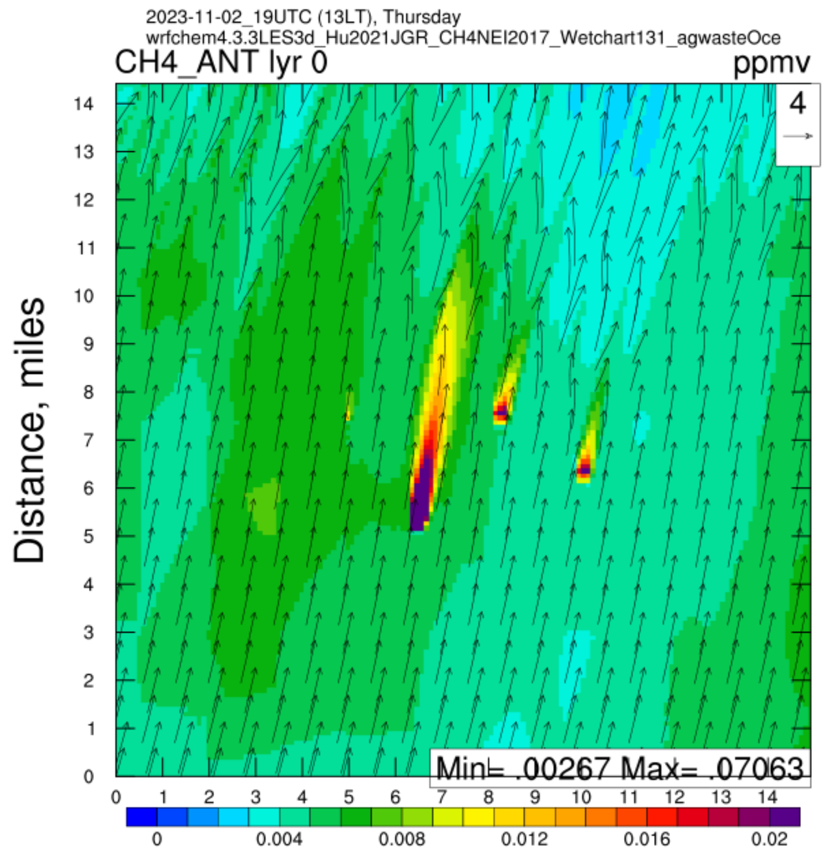


49,248*9 g/day at enlink site and 12,096*9 g/day at devon and El reno site

# References


1. **Hu, X.-M.**,Gourdji, S. M., Davis, K. J., Wang, Q., Zhang, Y., Xue, M., . . . Crowell, S. M. R. (2021). Implementation of improved parameterization of terrestrial flux in WRF-VPRM improves the simulation of nighttime CO2 peaks and a daytime CO2 band ahead of a cold front. *JGR: Atmospheres*, e2020JD034362. 10.1029/2020JD034362.
2. **Hu, X.-M.**, S. Crowell, et al. (2020), Dynamical Downscaling of $CO_2$ in 2016 over the contiguous United States using WRF-VPRM, a weather-biosphere-online-coupled model, *J. Adv. Modeling Earth Systems*, 10.1029/2019MS001875.
3. Li, X., **Hu, X.-M.**, Cai, C. et al. (2020), Terrestrial $CO_2$ Fluxes, Concentrations, Sources and Budget in Northeast China: Observational and Modeling Studies, *J. Geophys. Res.-Atmospheres*, 10.1029/2019JD031686.
4. **Hu, X.-M.**, J. Hu, L. Gao, C. Cai, Y. Jiang, M. Xue, T. Zhao, and S. M. R. Crowell, 2020: Multi-sensor and multi-model monitoring and investigation of a wintertime air pollution event ahead of a cold front over eastern China. J. Geophy. Res., Conditionally accepted.
5. **Hu, X.-M.**, and M. Xue (2016b), Influence of synoptic sea breeze fronts on the urban heat island intensity in Dallas-Fort Worth, Texas, *Mon. Wea. Rev.*, doi:10.1175/MWR-D-15-0201.1.
6. **Hu, X.-M.**, et al. (2014), Impact of the Loess Plateau on the Atmospheric Boundary Layer Structure and Air Quality in the North China Plain: A Case Study, Science of the Total Environment, 10.1016/j.scitotenv.2014.08.053
7. **Hu, X.-M.**, et al. (2013), Impact of the Vertical Mixing Induced by Low-level Jets on Boundary Layer Ozone Concentration, *Atmos. Environ.*, 70, 123-130
8. **Hu, X.-M.**, J. M. Sigler, and J. D. Fuentes (2010), Variability of ozone in the marine boundary layer of the equatorial Pacific Ocean , *J. of Atmos. Chem.*, 66, 117–136.